C.P. No. 654

C.P. No. 654

MINISTRY OF AVIATION

AERONAUTICAL RESEARCH COUNCIL

CURRENT PAPERS

The Calculation of the Velocity Distribution due to Thickness for Swept Wings with Subsonic Edges at Supersonic Speeds

By

A.B. Haines, K. Rollins and J. Osborn

LONDON: HER MAJESTY'S STATIONERY OFFICE

1964

TEN SHILLINGS NET

C.P. No.654

June, 1962

The Calculation of the Velocity Distribution due to Thickness for Swept Wings with Subsonic Edges at Supersonic Speeds

- By -

A. B. Haines,
K. Rollins
and J. Osborn

SUMMARY

This note describes a method for calculating according to linearised theory, the velocities produced by the thickness form of a sweptback wing having subsonic leading and trailing edges at supersonic Mach numbers. The method has been programmed for the Zebra computer and can cope with wings of arbitrary planform having arbitrary variation of both thickness/chord ratio and section shape across the span. At present, the method will only deal with wings having sharp leading edges. It is likely, however, that for round-nosed sections, if the true section is replaced by an equivalent sharp-nosed section, reliable results may still be obtained, at least aft of about 0.04c.

Calculations have been made for the velocities due to thickness at M = 1.2 over four different wings. These are respectively, untapered, tapered in plan, tapered both in plan and thickness/chord ratio and finally, tapered with a spanwise variation in section shape. In one case, a comparison with experimental results is given.

The results for the fourth wing show that the changes in velocity produced by changes in thickness shape near the root are qualitatively similar at supersonic and at subsonic speeds. This is an important result and it follows that in certain applications, changes in section shape could be used to reduce the required amount of body waisting while in general, allowing the section shape to vary spanwise should give an added freedom in designing a suitable body shape to meet the requirements of the isobar patterns over both the upper and lower surface.

Replaces A.R.A. Wind Tunnel Note No. 43 - A.R.C.23,976.

List of Contents

List of Figures

1. INTRODUCTION

This note is a contribution to the already extensive literature dealing with the design of sweptback wings and the calculation of the pressure distributions over them in subcritical-type flow before any strong shock waves are present on the wing surface. In the past, the design cruising speed for most applications has been below $M = 1.0$ and even probably below say, $M = 0.92$. It has been shown however, e.g., in reference 1, that subcritical-type flow can be maintained over a sweptback wing at a supersonic free-stream Mach number provided that the wing sweep and thickness are chosen appropriately, provided that the body is shaped to avoid a loss in sweep on the isobar pattern over the wing near the root and provided that a suitable planform is chosen for the wing tip region so as to eliminate the infinite singularity in the loading near the tip leading edge. A possible application for a sweptback wing of this type would be to a supersonic transport aircraft designed to cruise at $M = 1.15$, i.e., as fast as possible without producing a sonic bang. It follows that there is a need to develop methods for calculating the pressure distribution over such wings at supersonic flight speeds for which the wing leading and trailing edges are still subsonic.

For an infinite sheared wing - and hence possibly for the mid-semispan station of a finite sweptback wing - the extension of existing subsonic methods to a supersonic flight speed presents no problems. Also, relatively simple formulae are available, e.g., in reference 2, for calculating the pressure distribution at the actual centre or root section. In designing the wing-body combination however to give a good isobar pattern over both the wing upper and lower surface and to give reasonable flow over the body, it is not enough to know the pressure distribution at just these two stations on the wing. For example, in calculating the most appropriate body cross sectional shapes, one needs to know the velocities induced by wing thickness, camber and incidence at several stations across the span.

In the past when dealing with the problem at subsonic speeds, the complete linearised solution in incompressible flow was obtained wherever possible[3] but the method[4] in common use for calculating the velocities at subsonic speeds over a wing of arbitrary design was built up by linking the solutions for the sheared wing and for the root and tip sections by interpolation functions that were derived partly by analysis of results obtained for particular cases by the full linearised solution and partly by analysis of available experimental data. This sort of approach was dictated initially by the fact that high speed digital computers were not generally available at the time and so simplified methods had to be developed which could be handled with desk machines. The position is now however completely different and so it seems appropriate to abandon this approach and to tackle the supersonic problem by trying to develop methods for calculating the velocities at any point over the surface of a wing of arbitrary geometry. It is still only practicable to use linearised theory and one must expect that as at subsonic speeds, comparison with experiment may later dictate some amendments to the theoretical results in order to improve on linearised theory.

The present note is intended to fit in to this general framework. It describes a method for calculating for supersonic speeds, the velocities due to the thickness form of a sweptback wing with subsonic leading and trailing edges. It must be stressed at the outset that it does not deal with the inverse problem of finding the thickness distribution for a wing to satisfy a specified pressure distribution. This would be the normal design problem but at the moment, it has to be tackled by the present method, arriving at the required shape by an iterative approach. The method is designed to cope with wings with an arbitrary planform and with the thickness/chord ratio and with the thickness form varying spanwise in an arbitrary manner. All that is necessary is for the wing leading-edge and the spanwise variation in local section slope to be expressible in polynomial form. The main restriction is that the method is so far applicable only to wings with

sharp/

sharp leading edges. For round-nosed sections, it is suggested that a fair approximation can be obtained by modifying the section close to the leading edge to give an equivalent sharp-nosed section. A comparison with exact linearised theory for round-nosed sections has not yet been possible but the present approach should be regarded as merely temporary; ultimately, the aim will be to provide the exact linearised solution. The first part of the note is concerned with the evaluation of the double integral involved in deriving the potential from the second-order differential equation. Particular reference is made to the methods used for coping with the fact that the integrand becomes infinite at the point for which the potential is being calculated and along the forward Mach-lines through this point. It is worth noting here that as with the subsonic methods of references 3 and 4, the method initially gives the velocity distributions in the chordal plane but suggestions are made as to how then to derive the velocity distribution over the surface by using an approximation which strictly can only be justified for a two-dimensional wing of elliptical cross-section. The extension to the three-dimensional case seems however to be logical and there is no reason to doubt that the results should be reasonably plausible. The full method has been programmed for the Stantec Zebra computer and an indication of the actual computer programme is given in Appendix I.

In the later part of the note, results calculated by this method are presented for four different wing designs. The first is a simple untapered sweptback wing for which a comparison is possible with the results of other calculations. This example therefore affords some check on the methods used and on the accuracy of the computer programme. The second wing is tapered in planform and for this case, comparisons are made with some experimental results. In the third example, the wing is both tapered in planform and in thickness/chord ratio while in the fourth example, the wing section shape varies across the span. This last example is intended mainly to show that the programme is capable of tackling such a wing and to illustrate that this design feature may prove useful at supersonic speeds in the same way as it has been in the past at high subsonic speeds.

2. GENERAL OUTLINE OF METHOD

The starting point is to solve the three-dimensional linearised potential equation for inviscid, compressible supersonic flow:

$$\beta^2 \frac{\partial^2 \phi}{\partial x^2} - \frac{\partial^2 \phi}{\partial y^2} - \frac{\partial^2 \phi}{\partial z^2} = 0 \qquad \ldots\ldots\ldots (1)$$

$$\text{where} \quad \beta^2 = M_o^2 - 1$$

(x,y,z) are a system of rectangular coordinates such that x is measured in the free-stream direction, y spanwise and z normal to the chordal plane. The origin of the axes is at the leading edge of the centre section, V_o is the free-stream speed and M_o, the Mach number of the free stream.

It is known that equation (1) has a solution of the form

$$\phi = -\frac{1}{2\pi} \iint_{\sigma} \frac{q(X,Y)\, dX\, dY}{\sqrt{(x-X)^2 - \beta^2 (y-Y)^2}} \qquad \ldots\ldots\ldots (2)$$

where $q(X,Y)$ is the source strength at the point (X,Y) and where

$$q(X,Y) = 2V_o \left(\partial z/\partial x\right)_{X,Y} \qquad \ldots\ldots\ldots (3)$$

In arriving at this solution, one has made several of the usual assumptions of linearised theory for thin aerofoils, e.g., that the velocity

increment/

increment v_x is small compared with the free-stream speed V_o, and that the vertical component, v_z, is determined on the chordal plane, $z = 0$, instead of on the surface. Substituting (3) in (2) gives

$$\frac{\phi}{V_o} = -\frac{1}{\pi}\iint_o \frac{(\partial z/\partial x)_{X,Y}\, dX\, dY}{\sqrt{(x-X)^2 - \beta^2(y-Y)^2}} \qquad \ldots\ldots\ldots (2a)$$

Then $$\frac{v_x}{V_o} = \frac{\partial}{\partial x}\left(\frac{\phi}{V_o}\right) = \frac{\partial}{\partial x}\left\{-\frac{1}{\pi}\iint_\sigma \frac{(\partial z/\partial x)_{X,Y}\, dX\, dY}{\sqrt{(x-X)^2 - \beta^2(y-Y)^2}}\right\} \qquad \ldots\ldots\ldots (4)$$

and similarly for v_y/V_o.

The crux of the problem is to obtain a method for the accurate numerical evaluation of the double integral (2a). The surface σ in the chordal plane over which this integration has to be performed is the portion of the wing area ahead of the forward Mach-lines through the point (x,y) at which the potential is required (see Figure 1). In addition to becoming infinite at this point (x,y), the integrand in (2a) also becomes infinite at points along the Mach-lines,

$$(x-X) = \pm\beta\,(y-Y) \qquad \ldots\ldots\ldots (5)$$

through (x,y) and unless the aerofoil has a sharp nose, it will become infinite at the wing leading edge since dz/dx equals infinity there. This last problem is not tackled in the present analysis which is restricted to sharp-nosed sections but satisfactory methods have been developed as described below in section 3 for dealing with the other singularities.

After integrating and then differentiating by (4) to give the incremental velocity components, v_x/V_o and v_y/V_o, the velocities on the chord-line are given by

$$\left\{\frac{V(x,y,o)}{V_o}\right\}^2 = \left(1 + \frac{v_x}{V_o}\right)^2 + \left(\frac{v_y}{V_o}\right)^2 . \qquad \ldots\ldots\ldots (6)$$

On the wing centre-line, by symmetry, $v_y/V_o = 0$. Also for this section, one can convert to the velocity at a point on the surface, using the approximate relation

$$\left(\frac{V(x,y,z)}{V_o}\right)^2 = \frac{(V(x,y,o)/V_o)^2}{1 + (\partial z/\partial x)^2_{x,o}} . \qquad \ldots\ldots\ldots (7)$$

This relation is rigorously true for a two-dimensional wing of elliptic section, i.e., for $v_y = 0$.

If v'_x/V_o is the velocity component at a point (x,o,z) on the surface, equation (7) can be rewritten as

$$\frac{v'_x}{V_o} /$$

$$\frac{v'_x}{V_o} = \frac{1 + (v_x/V_o)}{\sqrt{1 + \left(\frac{dz}{dx}\right)^2_{x,o}}} - 1 \qquad \ldots\ldots\ldots (7a)$$

For points off the wing centre-line, the conversion process is more complicated and there is some uncertainty in what is the appropriate value for the term in the denominator. The suggestions made below appear however to be sound in principle. The first step is to resolve the velocity-components, v_x and v_y into components parallel and normal to a line making an angle ψ to the free-stream where

$$\tan \psi = - v_y/v_x .$$

For an infinite sheared wing, $\psi = \phi$ and so then, the velocities are being resolved into directions normal and parallel to the wing leading edge. By analogy with the equation which would apply in that limiting case, one can write

$$\left(1 + \frac{v_x}{V_o}\right)^2 + \left(\frac{v_y}{V_o}\right)^2 = \sin^2 \psi + \left(\cos \psi + \frac{v_\psi}{V_o}\right)^2$$

where $\frac{v_\psi}{V_o}$ is the component in a direction making an angle ψ with the free-stream.

It would then seem appropriate to use the surface slope measured in this direction in the term in the denominator of the expression for translating the velocity from the chordal plane to the surface. This slope, $(dz/dx)'$, is given by the relation

$$\left(\frac{dz}{dx}\right)' = \frac{dz}{dx} \cos \psi - \frac{dz}{dy} \sin \psi$$

$$= \frac{dz}{dx} \cdot \frac{\cos (\phi - \psi)}{\cos \phi} .$$

Then the equation for converting to the resultant velocity V' at a point (x,y,z) on the surface is as follows:

$$\left(\frac{V'}{V_o}\right)^2 = \sin^2 \psi + \frac{\left(\cos \psi + \frac{v_\psi}{V_o}\right)^2}{1 + \left(\frac{dz}{dx} \cos (\phi - \psi) \sec \phi\right)^2}$$

$$= \sin^2 \psi + \frac{\left\{\left(1 + \frac{v_x}{V_o}\right)^2 + \left(\frac{v_y}{V_o}\right)^2 - \sin^2 \psi\right\}}{1 + \left(\frac{dz}{dx} \cos (\phi - \psi) \sec \phi\right)^2} \qquad \ldots\ldots\ldots (8)$$

For/

For many applications, it should be possible to ignore $\left(\frac{v_y}{V_o}\right)^2$ and equation (8) then reduces to

$$\left(1 + \frac{v'_x}{V_o}\right)^2 = \sin^2\psi + \frac{\left\{\left(1 + \frac{v_x}{V_o}\right)^2 - \sin^2\psi\right\}}{1 + \left(\frac{dz}{dx}\cos(\phi-\psi)\sec\phi\right)^2} \quad \ldots\ldots\ldots (8a)$$

which reduces to (7a) when $\psi = 0$. When $\psi = \phi$, i.e., for the infinite sheared wing,

$$\left(1 + \frac{v'_x}{V_o}\right)^2 = \sin^2\phi + \frac{\left[\left(1 + \frac{v_x}{V_o}\right)^2 - \sin^2\phi\right]}{1 + \left(\frac{dz}{dx}\sec\phi\right)^2} \quad \ldots\ldots\ldots (8b)$$

If $\left(\frac{v_x}{V_o}\right)^2$ is also ignored, equation (8a) reduces to

$$2\frac{v'_x}{V_o} = \frac{2\frac{v_x}{V_o} + \cos^2\psi}{1 + \left(\frac{dz}{dx}\cos(\phi-\psi)\sec\phi\right)^2} - \cos^2\psi \quad \ldots\ldots\ldots (8c)$$

As noted above, equations (8) with $\psi = 0$ reduce to the correct limit for the centre section; also, with $\psi = \phi$, they reduce to the same expression for the infinite sheared wing as that recommended in reference 4 for use at subsonic speeds. This was obviously desirable. Since we are merely concerned with wings with subsonic leading edges, the conversion to the velocity on the surface should obviously be the same for an infinite sheared wing irrespective of whether the free-stream Mach number is less than or greater than 1.0.

The various steps in the calculation and the problems involved are discussed in more detail in the succeeding sections.

3. ANALYTIC MANIPULATION OF THE DOUBLE INTEGRAL

As mentioned above, the potential ϕ at an arbitrary point (x,y) on the wing is given by relation (2a) where the double integration is carried out over the area σ, ahead of the forward Mach-lines through the point (x,y). Assuming that we are merely dealing with wings with sharp leading edges, i.e., that dz/dx remains finite within the range of integration (see section 6), the integrand merely becomes infinite at the point (x,y) and for points along these forward Mach-lines. The field of integration is therefore divided into five parts σ_i $(i = 1, 2 \ldots 5)$ as shown in Figure 1. σ_1 is the area containing no singularity (assuming $\partial z/\partial x$ remains finite); $\sigma_{2,3,4}$ are narrow strips of width δ lying ahead of the Mach-lines and σ_5 is the part of these strips lying adjacent to the point (x,y) itself; σ_5 extends from $(y-\varepsilon)$ to $(y+\varepsilon)$ - see Figure 1.

Let/

Let $$\frac{(\partial z/\partial x)_{X,Y}}{\sqrt{(x-X)^2 - \beta^2 (y-Y)^2}} = F(X,Y)$$

then $$\frac{\phi}{V_o} = -\frac{I}{\pi} = -\frac{1}{\pi}\iint_{\sigma} F(X,Y)\, dX\, dY \qquad \ldots\ldots\ldots (2b)$$

In area o_1,

$$I_1 = \iint_{\sigma_1} F\, dX\, dY$$

$$= \int_{Y_a}^{Y_b} dY \int_{X_a}^{X_b} F\, dX \qquad \ldots\ldots\ldots (9)$$

where the limits of integration $(Y_a, Y_b;\ X_a, X_b)$ are as follows:

$$Y_a = \begin{cases} -s \\ \text{OR} \\ \text{the Y-coordinate of the point of intersection} \\ \text{(A on Figure 1) of } X = f_L^{-}(Y) \text{ and } (x-X) = \beta(y-Y) + \delta \end{cases}$$

whichever quantity has the smaller modulus

$$Y_b = \begin{cases} +s \\ \text{OR} \\ \text{the Y-coordinate of the point of intersection} \\ \text{of } X = f_L^{+}(Y) \text{ and } (x-X) = -\beta(y-Y) + \delta \end{cases}$$

whichever quantity has the smaller modulus

$$X_a = f_L(Y)$$

$$X_b = \begin{cases} f_T(Y) \\ \text{OR} \\ x - \beta(y-Y) - \delta \end{cases}$$

whichever quantity has the smaller modulus

$X = f_L(Y)$ is the equation of the leading-edge shape, with

$f_L^{+}(Y)$ for $Y > 0$ and $f_L^{-}(Y)$ for $Y < 0$.

$X = f_T(Y)$ is the corresponding equation for the trailing edge.

It should be noted that the integration with respect to X is performed first, contrary to methods which are developed from the theory for a two-dimensional aerofoil. This is to simplify the treatment for a wing of arbitrary planform; it is clear that a wing with a curved leading or trailing edge can be dealt with quite simply provided that the equations $f_L(Y)$ and $f_T(Y)$ can be expressed readily, e.g., in polynomial form.

Since there are no singularities in σ_1, relation (9) can be integrated between the specified limits by standard numerical procedures as described in section 4.

Turning/

Turning now to the areas $\sigma_{2\ldots5}$, the value of $(\partial z/\partial x)_{X,Y}$ in these areas is taken as constant and equal to the value at $(x - \beta|y - Y| - \frac{1}{2}\delta, Y)$ when carrying out the first integration with respect to X.

Let $X_o = x - \beta|y - Y| - \delta/2$

Then for the areas $\sigma_2, \sigma_3, \sigma_4$ (Figure 1), the first integral is solved as follows:

$$I' = \int_{x-\beta|y-Y|-\delta}^{x-\beta|y-Y|} F\, dX$$

$$= \left(\frac{\partial z}{\partial x}\right)_{X_o Y} \int_{x-\beta|y-Y|-\delta}^{x-\beta|y-Y|} \frac{dX}{\sqrt{(x-X)^2 - \beta^2 (y-Y)^2}}$$

$$= \left(\frac{\partial z}{\partial x}\right)_{X_o,Y} \left[\begin{matrix} - \\ + \end{matrix} \cosh^{-1} \left| \frac{x - X}{\beta(y - Y)} \right| \right]_{x-\beta|y-Y|-\delta}^{x-\beta|y-Y|}$$

$$\left(\begin{matrix} - \\ + \end{matrix} \text{ according to whether } \frac{x - X}{\beta(y - Y)} \begin{matrix} > \\ < \end{matrix} 0 \right)$$

$$= \left(\frac{\partial z}{\partial x}\right)_{X_o,Y} \cosh^{-1} \left\{ 1 + \frac{\delta}{\beta(y - Y)} \right\} \ldots\ldots (10) \left[y \begin{matrix} < \\ > \end{matrix} Y \right]$$

Hence for regions $\sigma_{2,\,3,\,4}$,

$$I_{2,3,4} = \int_{Y_{L_{2,3,4}}}^{Y_{U_{2,3,4}}} \left(\frac{\partial z}{\partial x}\right)_{X_o,Y} \cosh^{-1} \left\{ 1 + \frac{\delta}{\beta|y - Y|} \right\} dY \qquad \ldots\ldots (11)$$

where the limits of integration vary according to the region in question.

For σ_4,

$$Y_{L_4} = y + \varepsilon$$

and $Y_{U_4} = \left\{ \begin{matrix} s \\ \text{OR} \\ \text{Y-coordinate of point of intersection of} \\ X = f_L^+(Y) \text{ and } (x - X) = -\beta(y - Y) + \delta \end{matrix} \right.$ whichever quantity has the smaller modulus

For/

For o_2, o_3 there are two separate cases depending on whether the Mach-line $(x - X) = \beta(y - Y) + \delta$ intersects the x-axis ahead of or behind the wing trailing edge. If this point is $(x_c, 0)$ - see Figure 1, point C - the two cases for σ_2, σ_3 depend therefore on whether

$$x_c > 1 \quad \text{or} \quad x_c < 1$$

(since in all the analysis, the wing plan geometry is non-dimensionalised by the wing centre-line chord). i.e., case (a) : $1 - (x - \beta y - \delta) < 0$

case (b) : $1 - (x - \beta y - \delta) \geq 0$

In case (a),

$$Y_{L_2} = \begin{cases} -s \\ \text{OR} \\ \text{Y-coordinate of point of intersection of} \\ X = f_L^-(Y) \text{ and } (x - X) = \beta (y - Y) + \delta \end{cases} \quad \text{whichever quantity has the smaller modulus}$$

$$Y_{U_2} = \text{Y-coordinate of point of intersection of } X = f_T^-(Y) \text{ and } (x - X) = \beta (y - Y) + \delta$$

$$Y_{L_3} = \text{Y-coordinate of point of intersection of } X = f_T^+(Y) \text{ and } (x - X) = \beta (y - Y) + \delta$$

$$Y_{U_3} = y - \varepsilon$$

As before, $f_T^+(Y)$ is the equation of the trailing edge for $Y > 0$ and $f_T^-(Y)$ for $Y < 0$.

In case (b), regions 2 and 3 merge to become o_{23} and then

$$Y_{L_{23}} = \begin{cases} -s \\ \text{OR} \\ \text{Y-coordinate of point of intersection of } X = f_L^-(Y) \\ \text{and } (x - X) = \beta (y - Y) + \delta \end{cases} \quad \text{whichever quantity has the smaller modulus}$$

$$Y_{U_{23}} = y - \varepsilon$$

This/

This leaves region σ_5 around the point (x,y) itself. For this area

$$I_5 = \iint_{\sigma_5} F \, dX \, dY$$

$$= \int_{y-\varepsilon}^{y+\varepsilon} dY \int_{x-\beta|y-Y|-\delta}^{x-\beta|y-Y|} F \, dX$$

$$= \int_{y-\varepsilon}^{y+\varepsilon} \left(\frac{\partial z}{\partial x} \right)_{X_o,Y} \cosh^{-1} \left\{ 1 + \frac{\delta}{\beta|y-Y|} \right\} dY$$

$$\simeq -2 \left(\frac{\partial z}{\partial x} \right)_{x-\frac{1}{2}\delta,y} \int_{\varepsilon}^{o} \cosh^{-1} \left\{ 1 + \frac{\delta}{\beta(y-Y)} \right\} d\,(y-Y) \quad [y > \varepsilon]$$

$$= -2 \left(\frac{\partial z}{\partial x} \right)_{x-\frac{1}{2}\delta,y} \left\{ \left[(y - Y) \cosh^{-1} \left\{ 1 + \frac{\delta}{\beta(y-Y)} \right\} \right]_{y-\varepsilon}^{y} \right.$$

$$\left. + \int_{\varepsilon}^{o} \frac{\delta d(y-Y)}{\sqrt{2\beta\delta(y-Y) + \delta^2}} \right\}$$

$$= 2 \left(\frac{\partial z}{\partial x} \right)_{x-\frac{1}{2}\delta,y} \left\{ \varepsilon \cosh^{-1} \left\{ 1 + \frac{\delta}{\beta\varepsilon} \right\} + \frac{1}{\beta} \left[\sqrt{2\beta\delta\varepsilon + \delta^2} - \delta \right] \right\}$$

.... (12)

The total expression for ϕ is then given by

$$\frac{\phi}{V_o} = -\frac{1}{\pi} [I_1 + I_2 + I_3 + I_4 + I_5] \qquad .... (13)$$

$$\text{or} \quad -\frac{1}{\pi} [I_1 + I_{23} + I_4 + I_5 \quad] \qquad .... (13a)$$

according to whether $1 - (x - \beta y - \delta) < 0$

$$\text{or} \geqslant 0$$

with I_1 given by (9), I_2, I_3, I_4 by (11) and I_5 by (12).

For/

For a point on the wing centre-line, i.e., a point (x,0),

$$1 - (x - \beta y - \delta) \geq 0$$

and equation (13a) reduces to

$$\frac{\phi}{V_o} = -\frac{2}{\pi}\left[\int_o^{Y_{bo}} dY \int_{X_a}^{X_{bo}} \frac{(\partial z/\partial x)_{X,Y}\, dX}{\sqrt{(x-X)^2 - \beta^2 Y^2}}\right.$$

$$+ \int_\varepsilon^{Y_{u_{40}}} \left(\frac{\partial z}{\partial x}\right)_{X_{oo},Y} \cosh^{-1}\left\{1 + \frac{\delta}{\beta Y}\right\} dY$$

$$\left. + \left(\frac{\partial z}{\partial x}\right)_{x,o} \left\{\varepsilon \cosh^{-1}\left[1 + \frac{\delta}{\beta\varepsilon}\right] + \frac{1}{\beta}\left[\sqrt{2\beta\delta\varepsilon + \delta^2} - \delta\right]\right\}\right] \quad \ldots\ (13b)$$

where $Y_{bo} = \begin{cases} +X \\ \text{OR} \\ \text{the Y-coordinate of the point of intersection of} \\ X = f_L^-(Y) \text{ and } (x-X) = -\beta Y - \delta \end{cases}$ whichever quantity has the smaller modulus

$$X_a = f_L(Y)$$

$$X_{bo} = \begin{cases} f_T(Y) \\ \text{OR} \\ x + \beta Y - \delta \end{cases} \text{ whichever quantity has the smaller modulus}$$

$$X_{u_{40}} = \begin{cases} s \\ \text{OR} \\ \text{Y-coordinate of point of intersection of} \\ X = f_L^+(Y) \text{ and } (x-X) = \beta Y + \delta \end{cases} \text{ whichever quantity has the smaller modulus}$$

and $$X_{oo} = x - \beta Y - \delta/2.$$

It is worth noting at this point that a relatively simple expression can be derived for the supervelocity increment, v_x, at points on the centre-line of a wing, tapered in planform but having the same section shape throughout the span:

$$\frac{v_x}{V_o} /$$

$$\frac{v_x}{V_o} = -\frac{2}{\pi}\left[\left(\frac{dz}{dx}\right)\frac{1}{\sqrt{\tan^2\phi_X-\beta^2}}\log_e\frac{\tan\phi_X+\sqrt{\tan^2\phi_X-\beta^2}}{\beta}\right]_{x,o}$$

$$-\frac{2}{\pi}\int_o^x\left(\frac{dz}{dx}\right)_{(X,0)}\frac{\tan\phi_L-\tan\phi_T}{\tan^2\phi_X-\beta^2}$$

$$\left[1-\frac{\tan\phi_X}{\sqrt{\tan^2\phi_X-\beta^2}}\log_e\frac{\tan\phi_X+\sqrt{\tan^2\phi_X-\beta^2}}{\beta}\right]dX \quad \ldots\ (14)$$

In the first term, dz/dx and ϕ are both taken at the point (x,o); in the second term, both are functions of X. This expression is only valid if the centre-line section lies ahead of the Mach-line from the leading edge of the wing tip.

For the even simpler case of an untapered wing of sufficiently high aspect ratio, equation (14) reduces to

$$\frac{v_x}{V_o} = -\frac{2}{\pi}\left\{\frac{1}{\sqrt{\tan^2\phi-\beta^2}}\log_e\left(\frac{\tan\phi+\sqrt{\tan^2\phi-\beta^2}}{\beta}\right)\right\}\left(\frac{dz}{dx}\right)_{x,o}$$

$\ldots\ (14a)$

For wings having a more complex planform or thickness distribution, one has to revert to a numerical solution of equation (13b).

4. COMMENTS ON NUMERICAL EVALUATION OF ϕ AND $\partial\phi/\partial x$

This section is concerned with the numerical methods used for the evaluation of ϕ and $\partial\phi/\partial x$, the accuracy achieved and the time required on the Zebra computer. It should be emphasized that "accuracy" here refers merely to the numerical processes; the accuracy of the final results depends of course on other factors such as the assumptions of the linearized theory used in deriving the integral expressions in section 3 and the validity of the method used for transferring from velocities in the chordal plane to those on the wing surface. Also, if the wing section has a rounded leading edge, there is the practice of replacing the true section by an "equivalent" section having finite $\partial z/\partial x$ throughout. All these factors will be borne in mind when assessing the results of the calculations for specific examples in section 5 but for the present, we are merely concerned with the numerical methods used in deriving ϕ and $\partial\phi/\partial x$. In this context, the accuracy of the computed results depends mainly on three factors: the choice of values for the small quantities δ and ε, the methods chosen for the numerical solution of $I_{1\ldots4}$ and the detail in which the surface is mapped, e.g., the number of integrating strips and the number of points for which values of ϕ and $\partial\phi/\partial x$ are obtained.

4.1 Choice of values for δ and ε

In practice it is found that the choice of suitable values for the small quantities δ and ε (Fig. 1) is defined within fairly close limits. On the one hand, if δ and ε are too small, the values obtained for I_1 are inaccurate since the integrand becomes large as (X,Y) approaches (x,y). On the other hand, an upper limit on the possible values of δ and ε is set by the derivation of equation (12) for I_5 for points in the vicinity of the leading edge. This is illustrated by the sketch in Figure 2. For given values of δ and ε, the point (x_o,y) defined as shown in Figure 2 is the nearest point to the leading edge for which relation (12) for I_5 remains valid. For the points closer to the leading edge, the limits of the area of integration, c_5, would no longer apply. From Figure 2, it will be seen that

$$x_o = \varepsilon \tan \phi_L + \beta\varepsilon + \delta$$

If we put $\varepsilon = \delta$ for convenience,

$$x_o = \varepsilon (\tan \phi_L + \beta + 1)$$

i.e.,
$$\delta = \varepsilon = \frac{x_o}{\tan \phi_L + \beta + 1} \qquad \ldots\ (15)$$

Hence, if the aim is to obtain accurate values of ϕ and $\partial\phi/\partial x$ at points distant only x_o downstream of the leading edge, the maximum permissible values of δ and ε are given by (15).

While it is true that in practice, a much more serious consideration near the leading edge may be inaccuracies resulting from the relatively large values of $\partial z/\partial x$ of either the true or "equivalent" sections, this is really no justification for introducing another source of error and so it seems fair to take note of condition (15) when choosing values for δ and ε.

From experience gained in computing the results for the examples of section 5, it seems that in general, reliable values of I_1 can be obtained if

$$\delta = \varepsilon = 0.001.$$

For $M = 1.2$, $\phi_L = 55°$, using these values with equation (15) implies that results can be obtained for points that are not nearer the leading edge than 0.005 (all these values are in terms of the chord). It should be pointed out however that the values which are acceptable for δ and ε in any given case depend on the values of d^2z/dx^2 and $d^2z/dx\,dy$, since $d^2z(x',y')/dx^2$ is replaced by its value at the particular point $(x-\frac{1}{2}\delta, y)$. This means that strictly, the values of δ and ε should be reduced as one approaches the leading edge where dz/dx will be changing more rapidly with x and y. This is therefore yet another reason why the results of calculations by the present method may be somewhat in error for points very close to the leading edge. Indeed, it would appear that if the velocities are required for points closer than 0.005, it may be very difficult to strike a suitable compromise for the values of δ and ε.

4.2 Numerical methods

The programmes originally written for the Stantec Zebra computer used both the Weddle and Hardy six-strip quadrature formulae, combined in the following manner:

$$\phi = \frac{1}{14}(9\,\phi_W + 5\,\phi_H) \qquad \ldots\ (16)$$

where ϕ_W = value of ϕ obtained from the Weddle formula,

and ϕ_H = value of ϕ from the Hardy formula.

(Strictly, using the expressions in section 3, one evaluates ϕ/V_o but in this section, $1/V_o$ is omitted for convenience). This weighted mean of ϕ_W and ϕ_H is equivalent to the most accurate six-strip equal-interval formula, but uses simpler coefficients. Extensive tests of this programme were made,

including the calculation of ϕ for the untapered wing example quoted in section 5.1. When the values of ϕ were obtained merely for points at intervals of 0.1c along the chord at four spanwise stations, the method appeared to be satisfactory. Subsequently, however, calculations for points spaced more closely along the chord suggested that the ϕ-function was not smooth. As might be expected, this meant that the variation of $v_x = \partial\phi/\partial x$ along the chord was even more erratic and at some points, the changes in $\partial\phi/\partial x$ appeared to be discontinuous. Some of these apparent discontinuities could be genuine because they could correspond to the Mach-wave disturbances being propagated from the wing-root trailing edge or wing-tip leading edge, etc., but such explanations would not serve in the majority of cases. It seemed therefore that many of the erratic changes were spurious and were probably due to rounding errors in the numerical integration. Accordingly, the programme was rewritten using Gaussian quadrature which is the most accurate available for a given number of points arranged at an optimum non-equal spacing. In addition, the number of points in each integration strip was increased to sixteen, giving the following formula:

$$\int_x^{x+h} g(x)\,dx = \frac{h}{2} \sum_{i=1}^{8} a_i \left\{ g\left[x + \frac{h}{2}(1-x_i) \right] + g\left[x + \frac{h}{2}(1+x_i) \right] \right\} \qquad \ldots\ldots\ldots (17)$$

where a_i and x_i are tabulated in reference 5, h is the length of one integration strip and there are "n" such strips between the limits of I_1, I_2, I_{23}, I_3 and I_4 as set out in section 3.

4.3 Accuracy and computer time

Having established that relation (17) appears to provide the most reliable method of performing the numerical integrations, increasing accuracy should result from increasing "n", the number of integrating strips - but at the expense of computer time. With the present Simple-Code programme for Zebra, n = 10 has seemed to be a reasonable compromise. Checks made by doubling the number of strips, gave in general a change of ±5 in the fifth significant figure for ϕ and thus using n = 10, ϕ should be accurate to four significant figures.

The primary aim of course is to obtain values of $\partial\phi/\partial x$ and the values of ϕ have therefore to be differentiated. This could be done by the simple first difference formula:

$$\frac{\partial\phi}{\partial x} = \frac{\phi(x_i) - \phi(x_{i-1})}{x_i - x_{i-1}} \qquad \ldots\ldots\ldots (18)$$

or preferably by calculating second differences. The accuracy of $\partial\phi/\partial x$ thus depends not only on the computed values of ϕ but on the interval $h = (x_i - x_{i-1})$ between the points at which ϕ has been determined. A small interval tends to accentuate the rounding errors inherent in deriving ϕ by relations such as (17) and a large interval increases the inaccuracy of the approximation (18). In general, in making the calculations discussed in section 5, h was taken as 0.1 except for regions where $\partial\phi/\partial x$ was changing rapidly along the chord; in these regions, h was reduced to 0.05. If $\phi(x)$ were linear with x, as it would be near the maximum thickness, the maximum possible error in $\partial\phi/\partial x$ corresponding to an error of ±0.00005 in $\phi(x)$ would be ±0.001. This could represent about ±5% of $\partial\phi/\partial x$. The actual results in Figures 4, 6 and 10 for the different examples calculated do not seem to show a random variation as great as this and so the values may be pessimistic. On the other hand, it must be admitted that it is somewhat of an anticlimax to resort to these methods for obtaining $\partial\phi/\partial x$ and in future, it may be preferable to programme an

analytic/

analytic expression for $\partial\phi/\partial x$ rather than an expression for ϕ. This should improve the accuracy and also reduce the computing time involved.

To sum up, using the present method, a reasonable conclusion for a typical wing being designed for $M = 1.2$ is that use of a 10-strip, 16-point Gaussian integration should give an accuracy of the order of ±5%.*

The time required on the computer depends not only on the number of integrating strips but also on how complex is the wing geometry and on the spanwise and chordwise position of the point at which ϕ is being calculated. The existing Simple Code programme for Zebra, using the 10-strip Gaussian integration, is such that the times required to compute values of ϕ at different positions on the tapered, constant section wing B in section 5.2 were as follows:

Centre section

15 minutes at $x/c = 0.1$ to 2 hours at $x/c = 1.0$,

$\eta = 0.5$

$2\frac{1}{2}$ hours at $x/c = 0.1$ to 6 hours at $x/c = 0.8$.

If the number of integrating strips were increased to 20, the times would be increased by a factor of about 4. More complex wings such as wing C in section 5.3 require slightly longer times but this factor should not exceed 1.5.

Rewriting the programme in Normal Code should reduce the times to possibly 1/4 of those quoted. Ideally, however, the change to Normal Code should be used to give a sizeable reduction in the time, combined with an improved accuracy through an increase in the number of integrating strips.

These computer times are obviously very lengthy. It was possible to obtain the results for the four examples discussed below in section 5 by allowing the computer to run all night on this programme. Clearly, however, if any major amount of work was required in a short space of time, the programme would have to be transferred to a faster computer. This is a particularly important point in view of the fact that one is calculating the velocity distributions for a given wing geometry and that therefore, to design a wing to give a prescribed pressure distribution - the normal design problem - one has to adopt an iterative approach calculating the pressure distributions for a range of wing shapes. Perhaps the more important conclusion is that these computer times illustrate the drawback of performing a double integration numerically. It is quite feasible that the times would be reduced by an order if one of the integrations were performed analytically and if therefore the computer was only required to carry out a single numerical integration. It is hoped to adopt this approach in future when deriving a method for the general case including wings with round leading edges. This point is referred to again in section 6.

5. CALCULATED EXAMPLES

Calculations have been made for four wings. Their geometry is of steadily increasing complexity: the first is untapered and has the same section shape throughout the span; the second is tapered in plan; the third is not only tapered in plan but also has its thickness/chord ratio varying across the span while the fourth also incorporates a spanwise variation of section shape.

The/

*Further experience has shown that $n = 5$ integrating strips should be sufficient in most cases and therefore the computer times quoted in this section can be taken as being pessimistic by a factor of about 3.

The plan dimensions of the wings (e.g., in Figures 5, 8) are made non-dimensional in terms of the centre-line chord.* For the tapered wings, the parameter η defining the spanwise position of a section is related to the semispan of the corresponding arrowhead wing, i.e., for the tip section of the true wing, $\eta < 1.0$.

Wings 2-4 were specified as wing-body configurations but for the purpose of the present calculations, the body-side was assumed to act as a full reflection plate and so the pressures were computed for the nett wing, assuming the root section was the centre plane.

In the equations for the surface slopes $(\partial z/\partial x)_{X,Y}$ for the various wings, z and x are assumed to be non-dimensionalised with respect to the local chord with $x = 0$ at the local leading edge and $x = 1$ at the local trailing edge. This may appear obvious but is stressed here since except when determining $(\partial z/\partial x)_{X,Y}$, x is non-dimensionalised with respect to c_o rather than c and $x = 0$ at the apex of the wing.

5.1 Untapered 55° sweptback wing (wing A)

Calculations were first made for an untapered 55° sweptback wing having an aspect ratio of 2.0 and a thickness/chord ratio of 0.054. This was chosen as the first example because values of the velocity increment, v_x/V_o, for this wing had already been obtained analytically by Weber at R.A.E. (Equation 14a gives the analytic expression for the velocities on the centre line; the relations are considerably more complicated for sections off the centre-line.)

For this wing, $\phi_L = \phi_T = 55°$, $c_o = 1.0$ (by definition) and the semispan, $s = 1.0$. The wing section was a sharp-nosed section A having the same maximum thickness position (0.31c) as the R.A.E. 101 shape and having the same shape as R.A.E. 101 aft of the maximum thickness. It differs from the R.A.E. 101 shape ahead of the maximum thickness, being defined by the values of dz/dx given in Table I and Figure 3. It will be seen that very nearly, the extreme forward part of the section is a wedge. This section was chosen for the calculations because results for this wing with this section had already been obtained analytically at R.A.E., using equations similar to (14). The purpose of this example therefore was primarily to test the accuracy of the computer programme.

For the computation, one has to express (dz/dx) as a polynomial in x where x is the distance along the local chord expressed as a fraction of the local chord, i.e., $x = 0$ at the local leading edge and $x = 1$ at the local trailing edge. For this shape A and a thickness/chord ratio of 0.054 as for the present example, suitable equations were derived as follows:

For $0 < x < 0.31$,

$$\frac{dz}{dx} = -35.995\,x^5 + 39.806\,x^4 - 24.4689\,x^3 + 9.2168\,x^2 - 2.18544\,x + 0.25512$$

For/

---

*Hence the output from the computer is strictly ϕ/c_oV_o and when differentiating numerically, one should remember that

$$\frac{v_x}{V_o} = \frac{1}{V_o}\frac{\partial\phi}{\partial x} = \frac{c_o}{c}\left\{\frac{\partial(\phi/c_oV_o)}{\partial(x/c)}\right\}$$

For $0.31 \leq x < 0.76$,

$$\frac{dz}{dx} = 1.3425\,x^4 - 3.2680\,x^3 + 3.1567\,x^2 - 1.48047\,x + 0.24055$$

For $0.76 \leq x < 1.0$,

$$\frac{dz}{dx} = -0.04798\ . \qquad \ldots\ldots\ldots (19)$$

Calculations were made for two stations: $\eta = 0$ (the centre section) and $\eta = 0.3$ and for $M_o = 1.2$. The results are compared in Figure 4 with those obtained analytically by Weber. It will be seen that extremely good agreement is obtained for both stations. Incidentally, the values of v_x/V_o as plotted are those derived for the chordal plane; they have not been corrected to give the velocities over the surface.

The agreement shown in Figure 4 represents an important step forward. It provides a useful check that the methods proposed for coping with the singularities along the Mach-lines and for performing the numerical integrations are satisfactory. An untapered wing of constant section shape does not of course enable one to check all the mathematics but if any fundamental errors were being made, they should have been apparent in the results for even this simple example. It should be stressed however that the agreement shown in Figure 4 provides no check on whether the basic assumptions of the linearised theory are valid but it is encouraging to find that the solution for ϕ is quite well behaved even far forward on the sections and that v_x/V_o appears to be varying in a manner that is physically plausible.

5.2 Tapered sweptback wing (Wing B)

Calculations were next made for a tapered sweptback wing (B) with a thickness/chord ratio of 0.06 for which experimental data have been obtained in the 8 ft × 6 ft transonic tunnel at R.A.E. Farnborough. The plan geometry of this wing is shown in Figure 5. It will be seen that the basic leading-edge sweep is 59.25° but outboard of about 0.7 × gross semispan, the leading-edge sweep is increased to form the usual sort of curved-tip shape. The trailing-edge sweep is 40° throughout.

As noted earlier, the calculations have to be made for the nett wing assuming that the body side acts as a full reflection plane. For convenience, the wing root chord at the body side is taken as 1.0 and the plan geometry is non-dimensionalised in terms of this length as shown on Figure 5.

The non-dimensionalised co-ordinates of the leading edge over the curved part outboard of station $Y = 0.5417$ are given in Table II. The polynomial that was fitted to these values by the method of least squares was

$$f_L(Y) = 57.5232\,Y^3 - 109.9240\,Y^2 + 71.4511\,Y - 14.6769 \qquad \ldots\ldots\ldots (20)$$

Inboard of $Y = 0.5417$,

$$f_L(Y) = 1.68085\,Y\ . \qquad \ldots\ldots\ldots (20a)$$

The wing section on the model tested at R.A.E. was the true R.A.E. 101 shape with a thickness/chord ratio of 0.06. As already explained, the present method has not been adapted to cope with an infinite value of dz/dx at the leading edge and so the calculations were made for the approximate shape B as defined by the values of dz/dx in Table I and Figure 3. It will be seen that this shape B has surface slopes that are very close to those of the true R.A.E. 101 shape. Strictly, the differences extend back to 0.1c but in fact, are quite trivial aft of 0.05c as can be seen from Figure 3(a).

The polynomials used to define this shape B are as follows:

For $0 < x < 0.01$,

$$\frac{dz}{dx} = 1.10933 - 74.687\,x,$$

For $0.01 \leq x < 0.05$,

$$\frac{dz}{dx} = 128941.6\,x^4 - 19796.65\,x^3 + 1171.566\,x^2 - 34.4294\,x + 0.60811,$$

For $0.05 \leq x < 0.3$,

$$\frac{dz}{dx} = -285.355\,x^5 + 307.206\,x^4 - 133.6010\,x^3 + 29.7481\,x^2 - 3.79101\,x + 0.27635$$

For $0.3 \leq x < 0.76$,

$$\frac{dz}{dx} = 1.6504\,x^4 - 3.9679\,x^3 + 3.76859\,x^2 - 1.73363\,x + 0.27821$$

For $x \geq 0.76$,

$$\frac{dz}{dx} = -0.05373\ . \qquad \ldots\ldots\ldots (21)$$

Chordwise distributions of v'_x/V_o were calculated for $M_o = 1.2$ for four stations across the span: $\eta = 0.108$, the body side, i.e., the effective centre section, and $\eta = 0.216$, 0.323, 0.431 (see Figure 5). In addition to calculating the velocity distributions for the shape B regarded as an approximation to the true R.A.E. 101 shape, calculations were also made for the shape A used above for the untapered wing A. Results of the calculations for these two sectionsshapes are compared in Figure 6. It will be seen that for the root section, there is little difference between the two sets of results but further out on the span, the differences are significant not merely near the leading edge but back to and even beyond the maximum thickness position. Qualitatively, there is nothing surprising in this. Figure 7 shows for example that the comparison is very similar when one calculates the velocity distribution over these two shapes in two-dimensional flow at $M = 0$. Figure 7 also gives the velocity distribution for the round-nosed R.A.E. 101 section as calculated by the Weber method as set out for example in reference 4. This figure shows that the approximate shape B gives results in very close agreement with those for the true round-nosed section, even as far forward on the chord as 0.05c. A similar comparison for supersonic speeds is not yet available and so for the moment, one has to take this evidence at $M = 0$ as providing some reassurance that it is fair to compare the calculated results for shape B with those measured experimentally on a wing having the true R.A.E. 101 shape.

This comparison between calculated and experimental results is given in Figure 8. The measured values were obtained from tests in the 8 ft x 6 ft tunnel at R.A.E. Farnborough at both $R = 0.75 \times 10^6$ and 1.5×10^6 (based on the wing mean chord) and data are shown both for tests with natural transition and alternatively, with transition fixed artifically at 0.15c. It should be added that the measured results for the centre section were modified before being plotted so as to allow for the effects of the forebody. This was done by subtracting two sets of experimental points, viz., circular unwaisted body plus wing and circular unwaisted body alone. It was shown experimentally that the contribution of the forebody to the pressure distributions at the other stations was negligible. The results at the two test Reynolds numbers were the same and so no distinction is drawn when plotting the points.

It/

It will be seen that over the forward part of the chord (say, 0.1-0.2c), the agreement between calculation and experiment in Figure 8 is reasonably good particularly for the centre section but that further aft, the measured supervelocities lie appreciably below the predicted values. The agreement for the centre section is certainly as good as that shown in reference 6 for an untapered wing.

The discrepancies between the measured and calculated values over the rear part of the section could be at least partly due to the effects of a thick boundary layer. Admittedly, as noted above, there is no difference between the results obtained at $R = 0.75 \times 10^6$ and $R = 1.5 \times 10^6$ but this does not necessarily mean that boundary layer effects are insignificant. In tests on similar wings in the A.R.A. transonic tunnel at even $R = 3.5 \times 10^6$, it was shown that the addition of some vortex generators could materially alter the velocities over the rear part of the wing. This result combined with the evidence of some oil flow photographs confirm that in the absence of the generators, a relatively thick boundary layer may tend to form over the rear part of a wing with a highly swept trailing edge. Tests are now being made in various tunnels to show whether this characteristic is influenced by a large change of Reynolds number, e.g., from $R = 1 \times 10^6$ to $R = 15 \times 10^6$. As regards the aft part of the sections, therefore, nothing definite can be concluded from the comparison in Figure 8 as to whether the theoretical results are valid or not. It is however a little disturbing that as y increases, the region along the chord where there is the most significant discrepancy between the measured and calculated values tends to move forward, e.g., for $\eta = 0.22$, it is aft of the maximum thickness; for $\eta = 0.32$, it is near the maximum thickness and for $\eta = 0.43$, it is ahead of the maximum thickness. This fairly systematic trend suggests that possibly there is some feature in the real flow which is not being represented correctly within the limitations of linearised theory. It would however be wrong to exaggerate the discrepancies. For example, the maximum discrepancy in v'_x/V_o at a given (x,y) rarely amounts to more than about 0.01. Also, it should be noted that where the discrepancies occur, the variation in v'_x/V_o with y is usually relatively rapid. This means that an alternative way of interpreting the results is to say that the measured distribution for $\eta = 0.43$, for example, corresponds quite closely with what would be calculated for about $\eta = 0.39$. This difference in η amounts to about $0.06 \times$ semispan; looked at in this light, the discrepancies may not be too important for a practical application.

Quite apart from the possibility of viscous effects in the measured results, there are several possible weaknesses in the theoretical approach which could be leading to these discrepancies. For example, the fact that a fairly small change in the effective spanwise position could bring about a considerable improvement suggests that the assumption that the actual wing-body combination can be treated as a simple nett wing for the purposes of these calculations may be partly responsible. Also, one must not lose sight of the fact that the assumptions of linearised theory and that the flow is subcritical may just not be good enough for these calculations for $M = 1.2$. It has long been known for example that use of the simple linear-theory Prandtl-Glauert transformation for estimating the pressures over a wing at high subsonic speeds is not really accurate enough when judged in comparison with measured experimental results. In addition, the various uncertainties near the leading edge will all tend to become rather more significant as y increases, e.g., the fact that the R.A.E. 101 section has been replaced by shape B (although Figure 7 is reassuring on this point), the fact that one has to transfer from the velocities in the chordal plane to the velocities over the surface by relations (8) and the fact that the choice of suitable values of δ and ε becomes more critical near the leading edge - see section 4.1. It seems quite clear however that none of these points in themselves could be fully responsible for the discrepancies.

It/

It would however be quite wrong to over-exaggerate the discrepancies and it is too early to draw any conclusions as to the true explanation. The important point at the moment is that one should be greatly encouraged by the general similarity in shape of the measured and calculated distributions and in their variation with spanwise position. There is no doubt that the calculated results are sufficiently accurate for the method to be extremely helpful in designing suitable wing shapes.

Before leaving the discussion of Figure 8, there is one interesting point of detail in the distributions for $\eta = 0.43$ that calls for comment. The distribution does not appear to be particularly smooth near 0.35c. In earlier calculations on the computer, this trend was even more noticeable and the calculation of values of ϕ at a number of intermediate points only made matters worse. It was then found that the relations similar to (20) that were being used for $f_L(Y)$ inboard and outboard of $Y = 0.5417$ did not give continuity in the first derivative of $f_L(Y)$ at this point. The numerical coefficients in equation (20) were then modified to the values given on page 16 in order to provide this continuity and the calculated velocity distributions were then as shown in Figure 8. The interrelation of the velocity distribution near 0.35 - 0.4c at $\eta = 0.43$ with the shape of the leading edge near the start of the curved tip can be explained by the fact that the Mach-line from this point on the leading edge crosses the $\eta = 0.43$ station in that particular region. It seems therefore that to obtain smooth velocity distributions across the chord at any station, one must make sure that the equation to the leading-edge shape is continuous at least to the first order and probably to the second. It is clear that irrespective of what happens in the real flow, the geometry has to be defined very carefully in order to obtain accurate results by the present method. The real flow would probably be less sensitive to any discontinuities in geometry but even in the real flow, a Mach-wave disturbance or a shock wave would be propagated from any actual kink in the leading-edge shape.

The discussion has concentrated on whether the calculations have given accurate results or not. It is tempting to compare the results in Figures 4 and 6 for the section shape A to see what have been the effects of taper (and the associated changes in local sweep) on the velocities due to thickness. This comparison is however somewhat clouded by the fact that there have been simultaneous changes in the aspect ratio and thickness/chord ratio. At the root or effective centre section, the maximum velocities are obtained at about 0.8c for both wings but are about 25% higher for the tapered wing. Its increased thickness/chord ratio could account for about 10%; the remaining 15% is presumably an indication that the lower effective sweep near the trailing edge of the tapered wing (40° rather than 55°) has been the dominant factor. Further out on the wing, to judge from the results for $\eta = 0.3$ for the untapered wing in Figure 4 with those for $\eta = 0.323$ for the tapered wing in Figure 6, the maximum velocities appear to be slightly higher on the tapered wing. It must be stressed however that one should not draw any conclusions from these results regarding the merits or otherwise of tapered versus untapered wings. The choice would obviously depend considerably on structural considerations but quite apart from this, even the aerodynamic arguments would depend on the flow produced when body, lift and warp effects are included. Any conclusions based on thickness effects alone could be very misleading.

5.3 Tapered sweptback wing with spanwise variation in thickness/chord ratio (wing C)

The next example extends the scope of the calculations to include a further factor: a spanwise variation in the thickness/chord ratio. As explained in reference 7, it is likely that in practice, tapered sweptback wings will be designed to have a variation in C_L across the span. For such designs, the thickness/chord ratio would have to be varied across the span in order to obtain a satisfactory isobar pattern over both the wing and

lower/

lower surfaces under the design conditions. A tapered sweptback wing with this feature has been designed[8] by Newby at R.A.E. Farnborough for tests in the 8 ft x 6 ft transonic tunnel. This design was therefore selected as the next example on which to try the present method. The velocities due to wing warp and incidence at the design C_L had been calculated at the R.A.E. and also a suitable body shape had been designed. In designing this body shape, it was assumed that the velocities at the body side due to wing thickness could be estimated on the basis of the local sweep at any chordwise position and the local thickness, i.e., the effects of the spanwise variation in thickness/chord ratio were ignored and the effects of planform taper were assumed to be related merely to the variation in sweep from leading to trailing edge. Calculations of the velocities due to thickness using the present method were required to obtain the velocities due to thickness at other spanwise positions so that the full isobar pattern over the wing surfaces under the design conditions could be calculated and compared with experiment.

The plan geometry of this wing C is shown in Figure 9. It is broadly similar to the planform of the previous example considered in section 5.2. At the wing root, the leading-edge sweep is 60° while the trailing-edge sweep is 40° throughout the span. Once again, the layout is really a wing-body configuration but the present calculations are made for the exposed nett wing treating the side of the body as the wing centre plane. The local chord c, was defined by the relation

$$c = c_c \mu_1 (1 - \eta)$$
$$= 1.11114 \mu_1 (1 - \eta) \qquad \ldots\ldots\ldots (22)$$

where c_c is the centre-line chord of the gross wing, and η is the spanwise coordinate based on the corresponding gross arrowhead wing. Values of the parameter μ_1 for a series of values of η are given in Table III. A standard programme using the method of least squares was used to fit a polynomial to the values of μ_1 out to $\eta = 0.7$ (i.e., nearly to the tip of the true wing); outboard of this, linear interpolation was used. The resulting equations for the trailing-edge and leading-edge shape are as follows:

$$f_T(Y) = 1 + 0.8391 \, |Y|$$
$$f_L(Y) = f_T(Y) + 1.11114 \mu_1 (1 - \eta)$$

where $\mu_1 (1 - \eta) = 1.0008 - 1.3336\eta + 4.7076\eta^2 - 21.7559\eta^3 + 40.1944\eta^4 - 26.2304\eta^5$

for $\eta < 0.7$

and $\mu_1 (1 - \eta) = 0.1538 \left[\dfrac{0.7071 - \eta}{0.007071} \right]$ for $\eta > 0.7$

and $\eta = 0.1 + 0.8036 \, |Y| \qquad \ldots\ldots\ldots (23)$

Values of the thickness/chord ratio at different stations across the span are also given in Table III and the method of least squares was again used to give the following polynomials for the variation of t/c across the span:

For $\eta < 0.5$,

$$t/c = -0.528073 - 0.397691\eta + 0.065309\eta^2 - 0.593439\eta^3 + 1.178682\eta^4$$

For/

For $0.5 \leqslant \eta \leqslant 0.65$,

$$t/c = -1.538312 + 12.428499\eta - 26.670750\eta^2 + 18.691644\eta^3$$

For $0.65 \leqslant \eta$

$$t/c = 29.464718 - 90.270769\eta + 70.093665\eta^2 . \quad \ldots\ldots\ldots (24)$$

The section shape on the model was R.A.E. 100 which for a thickness/chord ratio of 0.10 is defined by the equation

For $0 < x < 0.75$

$$z = 0.148188 \sqrt{x\,(1 - x)} \left(1 - \frac{8}{9} x\right)$$

and for $0.75 \leqslant x < 1.0$,

$$z = 0.085564\,(1 - x) . \quad \ldots\ldots\ldots (25)$$

The corresponding equations for dz/dx are:

For $0 < x < 0.75$,

$$\frac{dz}{dx} = 0.148188 \left\{ \frac{1}{18} [9 - 42x + 32x^2][x\,(1 - x)]^{-\frac{1}{2}} \right\}$$

and for $0.75 \leqslant x < 1.0$,

$$\frac{dz}{dx} = -0.085564 \quad \ldots\ldots\ldots (26)$$

To eliminate the infinite value of $(dz/dx)_{x=0}$, the aerofoil shape was modified ahead of $x = 0.005$, according to the following equation:

For $0 < x < 0.005$,

$$\frac{dz}{dx} = 3.92397 - 1052.2082x + 94525.3x^2 . \quad \ldots\ldots\ldots (27)$$

It is worth noting that the true R.A.E. 100 section shape was only modified ahead of 0.5% of the chord whereas for shape B representing the R.A.E. 101 section on wing B in para. 5.2, the changes extended back to 0.10c. It follows that the comparison when available between the calculated and measured results for this wing C should provide a much more sensitive test of whether one can retain the true section shape up to a point very close to the leading edge. There is of course another way of looking at this: the limiting factor could be the value of $(dz/dx)_{x=0}$ that can be tolerated. The value for the modification used here for the R.A.E. 100 section is actually 3.9 as compared with 1.1 for shape B corresponding to R.A.E. 101. Hence, in the present case, the slope at the leading edge has been allowed to approach 70°.

The chordwise distributions of v'_x/V_o calculated for this wing at $M_o = 1.2$ are shown in Figure 10. Results have been obtained for the full extent of the chord aft of about 0.05c for four stations including $\eta = 0.1$ which corresponds to the side of the body. Additional values over the forward part of the chord were calculated for four extra stations to help in

a detailed interpolation of the velocity distribution over the surface. As mentioned above, no comparison with experiment can yet be made but at first sight, the results of the calculations appear quite plausible. The values of v'_x/V_o obtained even as far forward as 0.05c seem to be reasonable. Near mid-semispan, e.g., for $\eta = 0.5$, the results are similar in general shape to those that would be obtained for the R.A.E. 100 section in two-dimensional flow - in particular, the maximum supervelocity occurs in the region from 0.1c to 0.2c and this is in line with the results in two-dimensional flow where the maximum velocity occurs at 0.12c. It is also worth mentioning that the velocities calculated for the body side are very close to those initially assumed by Newby when designing this wing-body combination. This seems to suggest that in the present case, the effects on the velocities due to thickness at the body-side due to the spanwise variation in thickness/chord ratio are relatively small.

5.4 Tapered sweptback wing with spanwise variation in section shape (wing D)

As explained above, it proved possible with wing C to design a waisted body such that the isobar pattern over the wing surface should be reasonably satisfactory assuming that the calculations are giving a reliable indication of the flow that would actually occur in practice. In other words, the contributions from the waisted body and from the wing warp were sufficient to compensate for the changes with spanwise position in the velocities due to thickness (Figure 10). As can be seen, the maximum velocity due to thickness occurs at a position that varies from about 0.13c for $\eta = 0.6$ to about 0.25c for $\eta = 0.3$ to 0.65c for the body-side at $\eta = 0.1$. It is clear that even in this case, the waisted body is being asked to provide quite a sizeable contribution and experience in trying to design other efficient sweptback wing-body combinations has shown that it is often difficult within the various practical limitations of an aircraft layout to accept the severely indented shapes that are actually required according to calculation. Indeed, one main reason why the problem did not prove too difficult with wing C was that the basic section shape chosen for the wing gave a "sheared-wing" velocity distribution with the maximum velocity occurring far forward. The tendency to obtain a severely indented body shape would be more acute for wings having sections giving a roof-top pressure distribution for the sheared wing with the roof top extending back to say, 0.4 or 0.5c. For the range of applications where it is difficult in practice to indent the body as required by calculation, it is important to consider whether the body requirements can be eased by also modifying the wing section shape near the root. It will be recalled that the combination of these two ideas has been suggested in the past for wing-body combinations operating at high subsonic speeds[9,10]. It is not to be expected that modifying the wing sections can be thought of as a complete alternative to shaping the body; the hope is that using the two ideas together may result in the required body shapes being less extreme. There is therefore an obvious interest in seeing whether varying the wing section shape near the root will give similar results at supersonic speeds.

Even for the planform, wing loading and basic section shape assumed for wing C, a case can still be made for suggesting that a forward movement of the maximum thickness near the root could be helpful. It would not necessarily reduce the amount of body waisting required but it would make it easier to choose a shape which was compatible with the requirements for the upper and lower surfaces. R.A.E. calculations suggested that a suitable velocity distribution due to thickness at the body-side might be that shown in Figure 11 where it is compared with the distribution calculated for the constant-section wing C. It will be seen that this "required" distribution is actually much nearer to the sort of distributions that were obtained for the outboard stations on wing C. The required distribution implies that the maximum thickness at the root should be at about 0.05 - 0.06c. The modified root section actually selected for the varying-section wing D has its maximum thickness at 0.13c (Figure 12). This means that wing D cannot be

expected to give the required body-side velocity distribution due to thickness shown in Figure 11. Nevertheless, the change from the basic R.A.E. 100 shape should be quite sufficient to demonstrate in principle what can be achieved by modifying the section shape near the root in this manner.

The new root section shown in Figure 12 was obtained by modifying the polynomial for dz/dx so that a smooth variation along the chord was obtained with a maximum thickness position at 0.13c and still retaining the same thickness/chord ratio as before. The values of dz/dx for the modified section and for the original R.A.E. 100 shape are compared in Figure 13. The values on these figures are for a thickness/chord ratio of 0.10; for the calculations, the same values of t/c were used as for the previous example - see Table III. The values of dz/dx for the modified section were expressed by the following relations:

For $0 \leqslant x < 0.01$,

$$\frac{dz}{dx} = \frac{t/c}{0.10}\{8.47193 - 817.193x\}$$

For $0.01 \leqslant x < 0.05$,

$$\frac{dz}{dx} = \frac{t/c}{0.10}\{0.77024 - 72.3269x + 3077.50x^2 - 58860.1x^3 + 413630x^4\}$$

For $0.05 \leqslant x < 0.25$,

$$\frac{dz}{dx} = \frac{t/c}{0.10}\{0.19587 - 3.3292x + 21.5481x^2 - 68.756x^3 + 83.93x^4\}$$

For $0.25 \leqslant x < 0.65$

$$\frac{dz}{dx} = \frac{t/c}{0.10}\{0.06971 - 0.73276x + 1.6812x^2 - 2.0110x^3 + 1.001x^4\}$$

For $0.65 \leqslant x < 1.0$

$$\frac{dz}{dx} = -\frac{t/c}{0.10}(0.06849) \quad \ldots\ldots\ldots (28)$$

The original section shape was retained at and outboard of $Y = 0.56$: the station as shown in Figure 14 at which the forward Mach line from the wing root trailing edge intersects the wing leading edge. To obtain the section at intermediate stations, the values of dz/dx for a thickness/chord ratio of 10% for the modified root and R.A.E. 100 shapes were interpolated linearly and then multiplied by the thickness/chord ratio of the original design (as discussed in section 5.3). To put this mathematically, one can refer to Figure 14 and say that

$$\left(\frac{dz}{dx} \times \frac{0.1}{t/c}\right)_{X_1,Y_1} = \left(\frac{dz}{dx} \times \frac{0.1}{t/c}\right)_{X_1,0} + \frac{Y_1}{Y_2}\left[\left(\frac{dz}{dx} \times \frac{0.1}{t/c}\right)_{X_1,Y_2} - \left(\frac{dz}{dx} \times \frac{0.1}{t/c}\right)_{X_1 0}\right]$$

$\ldots\ldots\ldots (29)$

(As in other cases when determining dz/dx, x and X are non-dimensionalised in terms of the local chord.)

To make this quite clear, the linear interpolation was carried out assuming that the sections were 10% thick throughout; in fact, the thickness/chord

ratio/

ratio variation was as given in Table III and as a result, the spanwise variation in dz/dx on the surface of the wing was not linear. This was done so that the calculations could show the effect of a change in section shape whilst still retaining the same thickness/chord ratio variation as on the original wing. It should perhaps be pointed out that it would have been no more difficult to calculate the velocities for a wing with a linear or even a parabolic or higher order distribution of dz/dx itself and this might have been nearer to a practical design. The essential point here is that the interpolation to find the geometry of intermediate sections is most conveniently done in terms of dz/dx rather than z. For the interpolation adopted in the present case, the values of dz/dx and z for a station midway between the root section and where the modification fades out are shown in Figures 12 and 13.

The effect of the modified wing sections on the velocity distributions at the body-side ($\eta = 0.1$) and at the intermediate station ($\eta = 0.25$) are shown in Figure 15. The important conclusion is that the changes in velocity produced by the changes in thickness shape near the root, are qualitatively similar to those that would have been produced at subsonic speeds. As regards the velocities at the body-side, the trend shown in Figure 15 is undoubtedly in the right direction. For example, if one had been merely trying to obtain a fully swept isobar pattern over this particular wing design at zero lift, the change from the body-side distribution due to thickness for wing C to that obtained for wing D would clearly have reduced the amount of body waisting required. Also, in the context of the R.A.E. design for lifting conditions, the distribution for wing D is closer to the required distribution shown in Figure 11. As noted earlier, to obtain agreement with the "required" distribution, the maximum thickness would have to have been moved even further forward to 0.05 - 0.06c and also it seems that the thickness/chord ratio would have had to be increased further since the values of v'_x/V_o over the major part of the chord are about 0.02 higher for the required distribution than for the results obtained for wing D.

For the intermediate section half-way between the root and where the modification fades out, the results for wing D are less satisfactory. The calculations suggest that relatively high velocities would occur far forward near the leading edge. From what has been said earlier, it is possible that the calculations are not fully reliable in this region but even so, the nature of the results does not in itself imply that they are inaccurate. The section shape at this intermediate station (Figure 12) is clearly rather bluff and it is therefore not surprising that the calculations are predicting high velocities near the leading edge. Experience in designing wings for subsonic flow has shown that this is often one of the pitfalls in designing modified section shapes near the root. For example, in reference 10, it was found that to avoid a region of high suctions near the leading edge a little way out from the root, it was necessary to introduce an additional control station not very far from the root rather than allowing the modification to fade out gradually. Similarly, in the present case, the high supervelocities at $\eta = 0.25$ could no doubt have been avoided by the choice of a different interpolation procedure across the span for dz/dx.

While it is true that the present example may not be entirely satisfactory either in the manner in which the geometry was specified or in the results obtained, it has been sufficient to demonstrate that there is undoubted scope for section modifications of this sort on sweptback wings being designed for supersonic Mach numbers. It remains to be seen whether the calculation methods as at present developed are good enough to cope with the designs needed in practice.

It is perhaps worth reiterating what can be done with the existing programme. In the example just considered, the expression for $(dz/dx)_{X,Y}$ that was used in evaluating the double integral can be written in the form

$$\left(\frac{dz}{dx}\right)_{X,Y}$$

$$\left(\frac{dz}{dx}\right)_{X,Y} = \sum_{1}^{m} A_m Y^m \left\{ \sum_{1}^{n} a_n X^n + (B_o + B_1 Y) \sum_{1}^{n'} b_n X^n \right\} . \qquad \ldots\ldots\ldots (30)$$

It would be relatively simple to extend this to

$$\left(\frac{dz}{dx}\right)_{X,Y} = \sum_{1}^{m} A_m Y^m \left\{ \sum_{1}^{n} a_n X^n + \sum_{1}^{m'} B_m Y^m \sum_{1}^{n'} b_n X^n \right\} \qquad \ldots\ldots\ldots (30a)$$

or more simply

$$\left(\frac{dz}{dx}\right)_{X,Y} = \sum_{1}^{n} a_n X^n \sum_{1}^{m'} B_m Y^m \sum_{1}^{n'} b_n X^n \qquad \ldots\ldots\ldots (30b)$$

or to add extra terms of a similar character. Also, as in the example just considered, the equation for $(dz/dx)_{X,Y}$ need not remain the same throughout the span; different equations could be used inboard and outboard of several "control stations". The coefficients (a_n, b_n, A_m ....) in equations (30) are assumed to be purely numerical; they are not functions of either X or Y. It is quite likely that for a varying section wing in practice, the wing would be designed on the principle of straight generators between two control stations and that therefore the interpolation would be a function of z rather than dz/dx. This could mean that strictly to represent such a wing by equations of the above form, the coefficients (A_m, B_m ....) would have to be functions of X. This would somewhat add to the complication, it would not just be a case of writing another sub-routine for the computer programme because it would have changed the nature of the integrals $I_{2\ldots5}$ that were solved in section 3. The hope therefore is that relations of the form (30a) or (30b) can be used for any practical example. This is a reasonable hope since one can always for the purposes of the calculation, introduce a relatively large number of "control stations". By this device, it should be possible to approximate to the true wing geometry between say, Y_1 and Y_2 quite closely. An increase in the number of control stations does not alter the mathematics or the validity of the integrations; it merely adds to the time required on the computer.

To avoid confusion about this question of the required number of "control stations", it should be stressed that in talking about the possibility of a large number, one is merely referring to what <u>might</u> have to be done in certain cases to compute the velocity distribution. It does not follow that one would need a lot of control stations for the actual wing to give a good aerodynamic performance. The number required in practice would obviously vary from one application to another and would depend on a proper balance between aerodynamic design and structural requirements. In general, it seems that 2 or 3 on a wing may not be sufficient and that the ideal number may be 4 or 5.

6. <u>CONCLUDING REMARKS</u>

This note has described a method for calculating the velocities due to thickness at supersonic speeds for sweptback wings with subsonic leading and trailing edges and with a finite leading-edge radius. The method is designed to cope with wings of arbitrary planform and with an arbitrary distribution of wing thickness form across the span. The wing leading-edge

and/

and trailing-edge shape, the spanwise distribution of thickness/chord ratio, the chordwise distribution of dz/dx and the fairing between the values of dz/dx at different stations across the span all have to be expressed in polynomial form. Suitable expressions for dz/dx on a varying section wing are given in relations (30). These various polynomials need not apply over the whole span; appropriate relations can be used to define the wing geometry between different "control stations"; an increase in the number of stations merely means that extra time is required on the computer. If these stations are also control stations in the design of the wing, genuine "kinks" in the geometry of the wing design could exist at these points but if not, experience has shown that it is important not to introduce any further artificial "kinks" when determining the polynomials to specify the geometry for these calculations. In cases where the true wing design is continuous across a control station, it is important to preserve this continuity between the polynomials applying inboard and outboard of the station - continuity not merely in the parameter in question but also in its first and even its second derivative. This is particularly so in the case of the wing leading-edge equations.

The method has been programmed for the Zebra computer and calculations have been made for four different wing designs. For a simple untapered, constant-section wing, good agreement was obtained with the results of desk-machine calculations using analytical expressions. For a tapered, constant-section wing, a comparison was possible with experimental results from tests in the 8 ft × 6 ft transonic tunnel at R.A.E. Farnborough. While the agreement between the measured and calculated results is not perfect, there is a general similarity in the shape of the measured and calculated velocity distributions and in their variation with spanwise position. Any differences that exist are not necessarily due to deficiencies in the theoretical approach but may be partly due to viscous effects in the experimental results.

The two main drawbacks to the method as presented are that strictly, it can only cope with sharp-nosed sections and that the times required on the Zebra computer are very long. This last point is obviously important since if the method is to be used in helping to design a wing to satisfy a certain prescribed pressure distribution, calculations have to be made for a range of wing geometries and an iterative approach adopted. The time on Zebra could be reduced by writing a programme in normal code rather than simple code; also, the outline of the computer programme included in Appendix I should help in transferring the programme to a faster computer if required. Before contemplating either of these steps, however, it would be preferable to see whether the method could be recast so that one of the integrations could be performed analytically leaving only a single integration to be solved numerically. If this were possible, an enormous saving in time would result.

The fact that the method strictly is confined to wings with sharp-nosed sections means that when obtaining results for comparison with experimental data for a wing with a round-nosed section, the true section shape has to be modified close to the leading edge. Experience to date suggests that a very small modification may suffice, e.g., for one of the examples discussed in the present note, the modification only extended over 0.005c and the slope at the leading edge was allowed to approach 70°. It appears that this probably gave satisfactory results for points aft of 0.05c and it is possible that it was satisfactory even ahead of this. Hence the present method may not be as restrictive as appears at first sight. Even so, the current trends in wing section design are emphasising the need for methods which give accurate results for the velocities very close to the leading edge. In the long term, therefore, the method should be recast to cope with round-nosed sections. This should be perfectly possible since although the integrand in equation (2) then becomes infinite at the leading edge, the integral still remains bounded for typical aerofoil shapes (since these are closely elliptical and the singularity is then of order $1/\sqrt{x}$).

Quite/

Quite apart from the question of the singularity at a round leading edge, it must be realised that the method can be no more accurate than are the assumptions of linearised theory. When analysing results for sweptback wings at high subsonic speeds, it has been found that the simple Prandtl-Glauert transformation, i.e., the linearised transformation, is not good enough and second order expressions have had to be derived. Similar conclusions could well apply at supersonic speeds. Another illustration of where the assumptions of linearised theory could give rise to significant errors is that for these calculations, the zone of influence affecting the potential and velocity at a given point is defined by the area ahead of the forward Mach-lines related to the Mach number of the freestream whereas in practice, it should be the Mach number of the local stream. Other sources of inaccuracy may exist close to the wing leading edge (even if it is sharp), e.g., the assumption that the source strength is proportional to the local $(\partial z/\partial x)$, the relations (8) for translating the velocities in the chordal plane into velocities over the surface and finally, the choice of an appropriate area isolating the singularity round the point for which the potential is being calculated. These are however all points of detail and should not be overstressed.

It is clear that the general trends indicated by results using the present method should be reliable. In particular, the method is valuable in that it gives the velocities due to thickness for a wing of complex geometry with, for example, the section shape varying across the span. The calculations already made for such a wing (D) lead to the important conclusion that changes in velocity produced by changes in shape near the root are similar qualitatively at supersonic speeds to those that would occur at subsonic speeds. In certain applications, modifying the wing section shape near the root might reduce the amount of body waisting required to give a satisfactory isovar pattern. More generally, allowing the section shape to vary near the root should give a greater freedom in devising a design that is both efficient aerodynamically and yet satisfies the restrictions of a practical layout. In particular, it should help in designing a body shape that is compatible with the requirements for the flow over both the upper and lower wing surface under the design conditions. As with subsonic applications in the past, the maximum thickness would have to be far forward at the wing root and the spanwise change in shape near the root would have to be relatively rapid. Experimental results for such a wing that could be compared with calculations using the present method would be of great interest.

LIST/

LIST OF SYMBOLS

c_c	centre-line chord of a wing-body configuration
c_o	root chord of a wing-body configuration, taken as the basic centre-line chord of a nett wing for present calculations and used to non-dimensionalise the wing plan geometry
$F(X,Y)$	function defined in equation 2(b)
M_o	freestream Mach number
q	source strength
s	semispan
t/c	thickness/chord ratio
V_o	freestream velocity
v_x, v_y	supervelocity components (in chordal plane)
v'_x	supervelocity component at point on surface
$X,Y,Z)$ $x,y,z)$	rectangular coordinate system with x measured in the freestream direction, y spanwise and z normal to the chordal plane. The origin of the axes is at the leading edge of the centre section. In general, x,y,z are non-dimensionalized with respect to the root or effective centre-line chord, c_c. N.B. In determining dz/dx, x is taken from the local leading edge and both x and z are non-dimensionalized with respect to the local chord c.
X_a, X_b, X_u etc.	appropriate limits of integration for equations in section 3
x_o	coordinate of the nearest point to the leading edge at which the velocities can be calculated for given values of δ and ε (see equation 15)
δ, ε	small quantities as defined in Figures 1 and 2. Typical values of δ and ε that have been used for the present calculations are $\delta = \varepsilon = 0.001$
β	$\sqrt{M_o^2 - 1}$
η	the ratio of y/semispan of corresponding gross arrowhead wing
μ_1	parameter in the relation (22) for defining the chord of a tapered wing
ϕ	potential or angle of sweep
ϕ_L	leading-edge sweep
ϕ_T	trailing-edge sweep
ϕ_W, ϕ_H	values of ϕ obtained from either Weddell or Hardy quadrature formulae

σ/.

σ area of integration, divided into $\sigma_1, \sigma_2 \ldots \sigma_5$ as shown in Figure 1

ψ defined by the relation $\tan \psi = v_y/v_x$

(for an infinite sheared wing, $\psi = \phi$)

LIST OF REFERENCES/

LIST OF REFERENCES

No.	Author(s)	Title, etc.
1	A. B. Haines and J. C. M. Jones	Transonic tunnel tests on a 6% thick, warped 55° sweptback wing model. A.R.A. Wind Tunnel Note No.25. A.R.C.22,466. October, 1960.
2	A. Ferri	Elements of aerodynamics of supersonic flow. MacMillan, New York, 1949.
3	S. Neumark	Velocity distribution on straight and sweptback wings of small thickness and infinite aspect ratio at zero incidence. A.R.C. R. & M.2713. May, 1947.
	S. Neumark	Velocity distribution on untapered, sheared and sweptback wings of small thickness and finite aspect ratio at zero incidence. A.R.C. R. & M.2717. March, 1949.
	S. Neumark and J. Collingbourne	Velocity distribution on thin tapered wings with fore-and-aft symmetry and spanwise constant thickness ratio at zero incidence. A.R.C. R. & M.2858. June, 1951.
		Velocity distribution on thin tapered arrowhead and delta wings with spanwise constant thickness ratio at zero incidence. A.R.C. R. & M.3008. May, 1955.
	K. W. Newby	The effects of taper on the supervelocities on three-dimensional wings at zero incidence. A.R. C. R. & M.3032. June, 1955.
4	J. A. Bagley	Some aerodynamic principles for the design of swept wings. A.R.C.23,173. May, 1961.
5	-	Unpublished M.o.A. Report.
6	J. E. Rossiter	Pressure measurements at the centre of a 40° sweptback wing with R.A.E. 101/10 sections at zero incidence and transonic speeds. A.R.C. C.P.542. June, 1959.
7	K. W. Newby	The shape of a wing having elliptic spanwise loading at M = 1.0. A.R.C.20,621. June, 1958.
8	K. W. Newby	Some thoughts on wing design - M = 1.2 transport. Unpublished.
9	A. B. Haines	Wing section design for sweptback wings at transonic speeds. A.R.A. Wind Tunnel Note No.13. Journal of the Royal Aeronautical Society, Vol.61, p.238. April, 1957.
10	A. B. Haines	Calculations on the effects of drag at high subsonic speeds of changes in section shape and spanwise thickness distribution on a swept wing. Unpublished M.o.A. Report.

APPENDIX I/

APPENDIX I

Computer Flow Diagram for Constant Section Wing

A: y = 0 Case

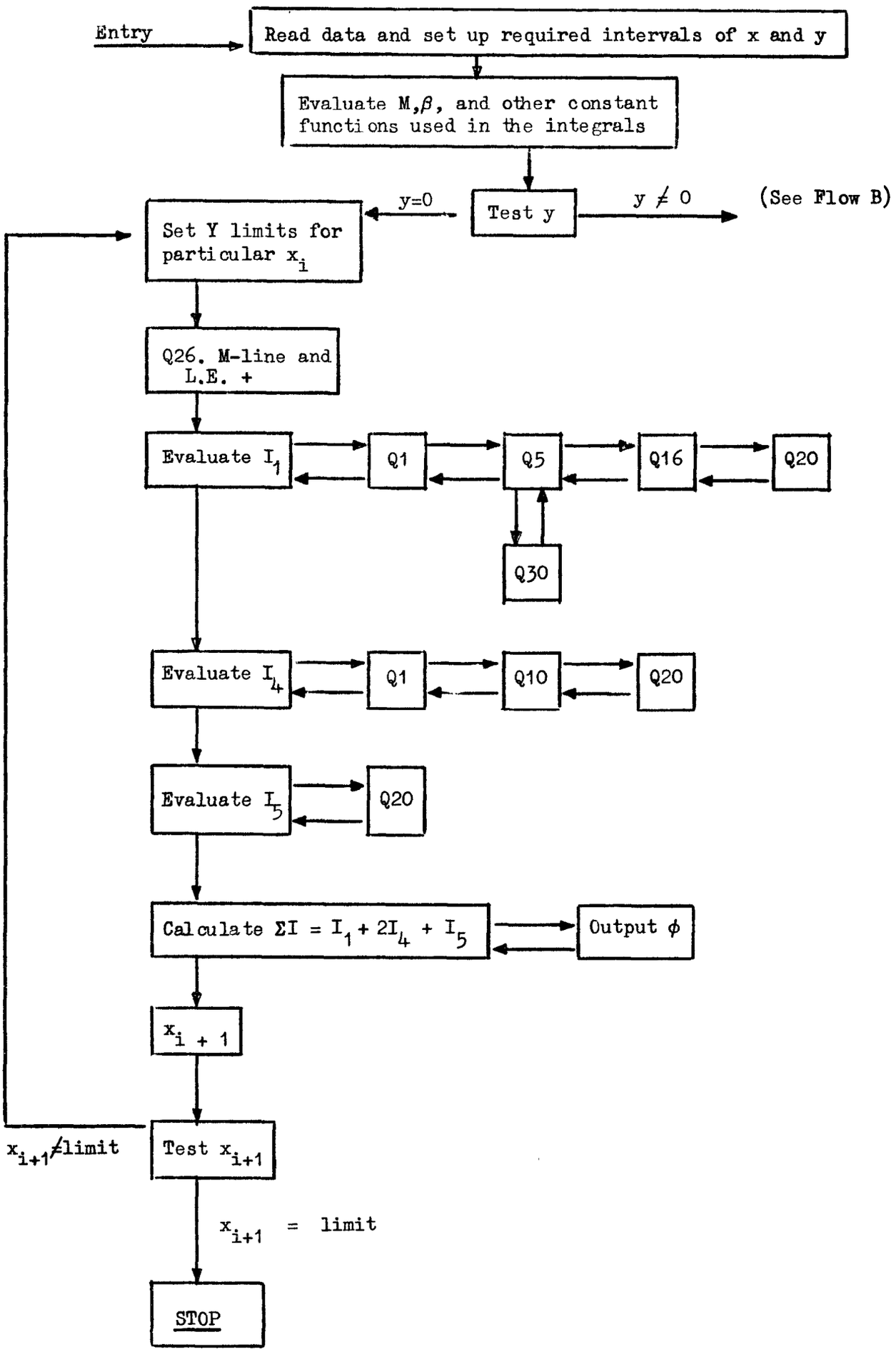

(N.B. Q subroutines listed after diagram B)

Computer Flow Diagram for Constant Section Wing

B: $y \neq 0$ Case

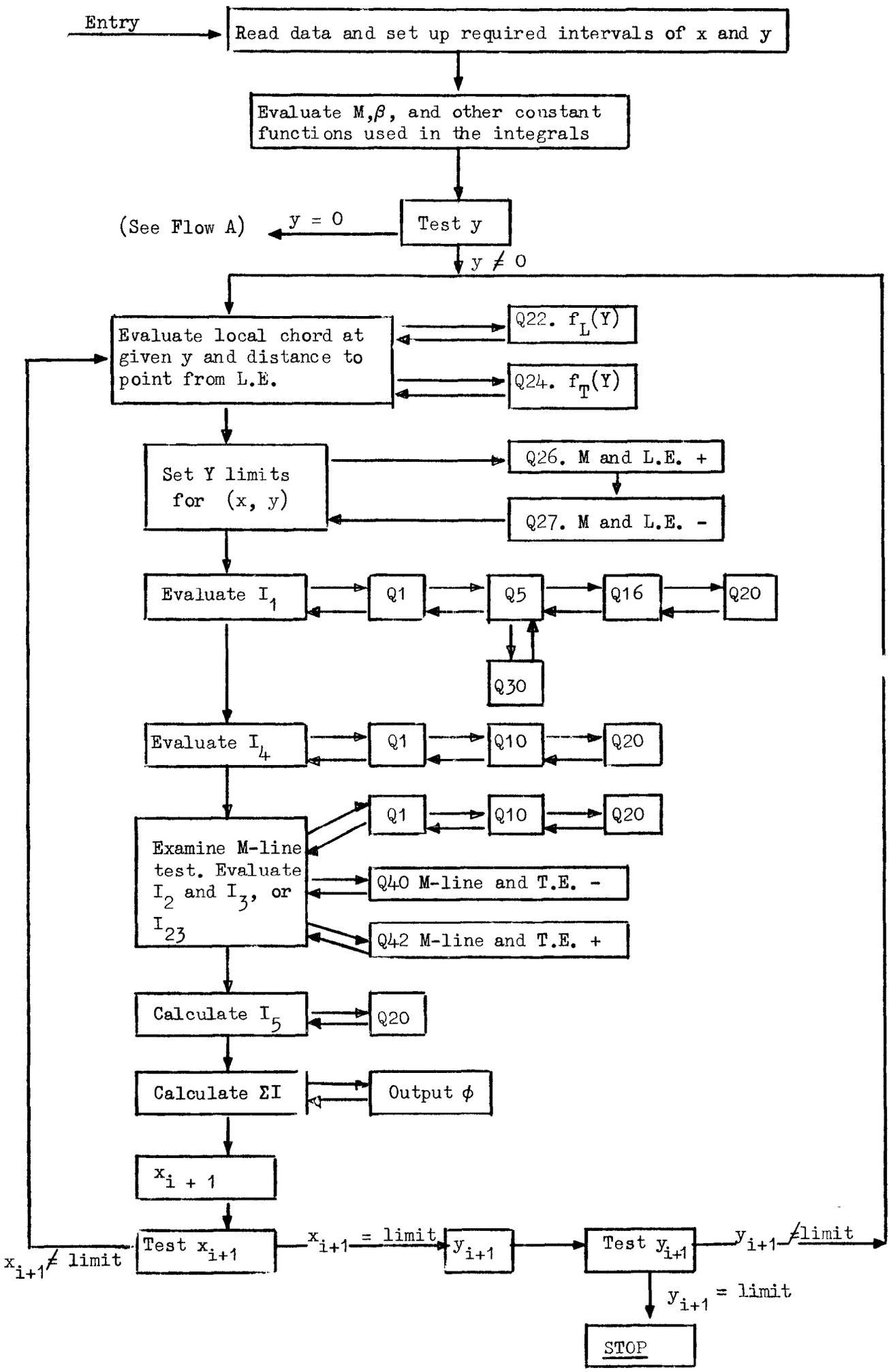

(N.B. Q subroutines listed below)

LIST OF Q SUBROUTINES USED IN COMPUTER PROGRAMME

1. FIXED SUBROUTINES

Q1 $\int dY$

Q5 $\int dX$

Q10 $\left(\frac{\partial z}{\partial x}\right) \cosh^{-1}\left\{1 + \frac{\eta}{\beta\,|y - Y|}\right\}$

Q16 $\dfrac{\left(\frac{\partial z}{\partial x}\right)_{X,Y}}{\sqrt{(x - X)^2 - \beta^2 (y - Y)^2}}$

Q30 $x - \beta\,|Y - y| - \delta$

OR: $f_T|Y| - x - \beta\,|Y - y| - \delta$

2. SUBROUTINES DEPENDENT ON WING GEOMETRY

Q20 $\left(\frac{\partial z}{\partial x}\right)_{X,Y}$ (Uses Q22 and Q24)

Q22 $f_L(Y)$

Q24 $f_T(Y) = |Y| \tan \phi_T + 1$

Q26 Intersection of M line and L.E. +

Q37 " " " " " L.E. -

Q40 " " " " " T.E. -

Q42 " " " " " T.E. +

TABLE I/

TABLE I

SECTION SHAPES USED FOR CALCULATIONS FOR WINGS A,B

$\frac{x}{c}$	$\frac{dz}{dx}$ SHAPE A	$\frac{dz}{dx}$ R.A.E.101	$\frac{dz}{dx}$ SHAPE B
0	0.4771	∞	1.8488
0.005	0.4571	0.8641	1.2265
0.010	0.4382	0.6041	0.6041
0.050	0.3107	0.2447	0.2438
0.100	0.2016	0.1489	0.1483
0.150	0.1304	0.1000	0.1000
0.200	0.0807	0.0656	0.0658
0.250	0.0433	0.0367	0.0362
0.300	0.0080	0.0063	0.0068

All the above figures correspond to a thickness/chord ratio of 0.10.

TABLE II

COORDINATES OF TIP LEADING-EDGE SHAPE FOR WING B (Fig.5)

Y_L	X_L
0.5417	0.9104
0.6223	1.0540
0.6702	1.1495
0.7180	1.2591
0.7659	1.3934
0.7898	1.4834
0.8138	1.6829

TABLE III

GEOMETRY OF VARYING t/c WING C

Planform given by $C = c_c \mu(1-\eta)$

η	t/c	μ
0	0.0528	
0.1000	0.0489	1.0000
0.1500	0.0468	
0.2000	0.0448	0.9996
0.2500	0.0428	
0.3000	0.0409	0.9974
0.3500	0.0389	
0.4000	0.0371	0.9901
0.4500	0.0357	
0.5000	0.0345	0.9684
0.5500	0.0339	0.9444
0.6000	0.0355	0.8999
0.6500	0.0405	0.8064
0.6750	0.0469	0.7103
0.6875	0.0537	0.6280
0.7000	0.0622	0.4734
0.707107		0

FIGS. 1 & 2.

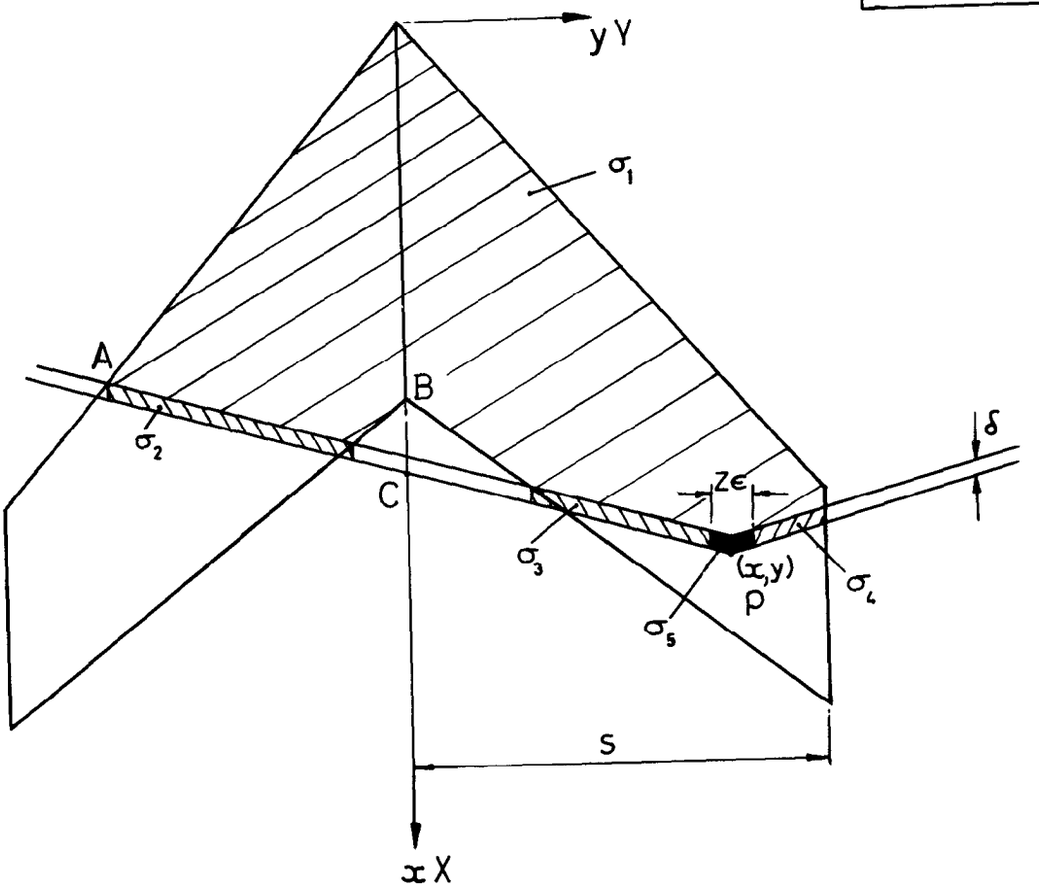

$$\sigma = \sigma_1 + \sigma_2 + \sigma_3 + \sigma_4 + \sigma_5$$

(IF C AHEAD OF B, $\sigma = \sigma_1 + \sigma_{23} + \sigma_4 + \sigma_5$)

FIG.1. FIELD OF INTEGRATION (σ) FOR DETERMINING POTENTIAL AT P (x, y)

(SEE § 3)

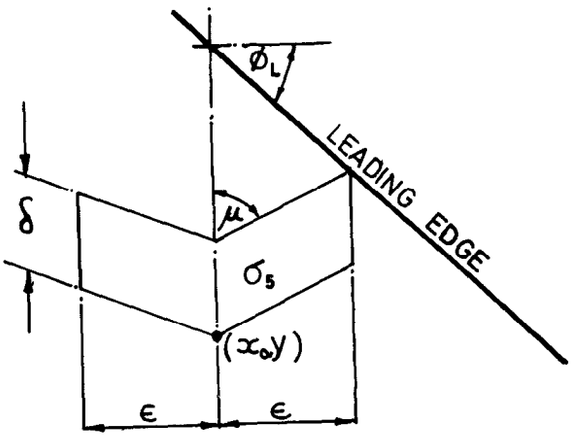

AREA σ_5 CANNOT EXTEND AHEAD OF LEADING EDGE THEREFORE ϕ CANNOT BE OBTAINED FOR POINTS AHEAD OF (x_0, y)

FIG.2. ILLUSTRATION OF HOW NEED TO DETERMINE POTENTIAL FOR POINTS NEAR L.E. CAN DICTATE CHOICE OF ϵ δ

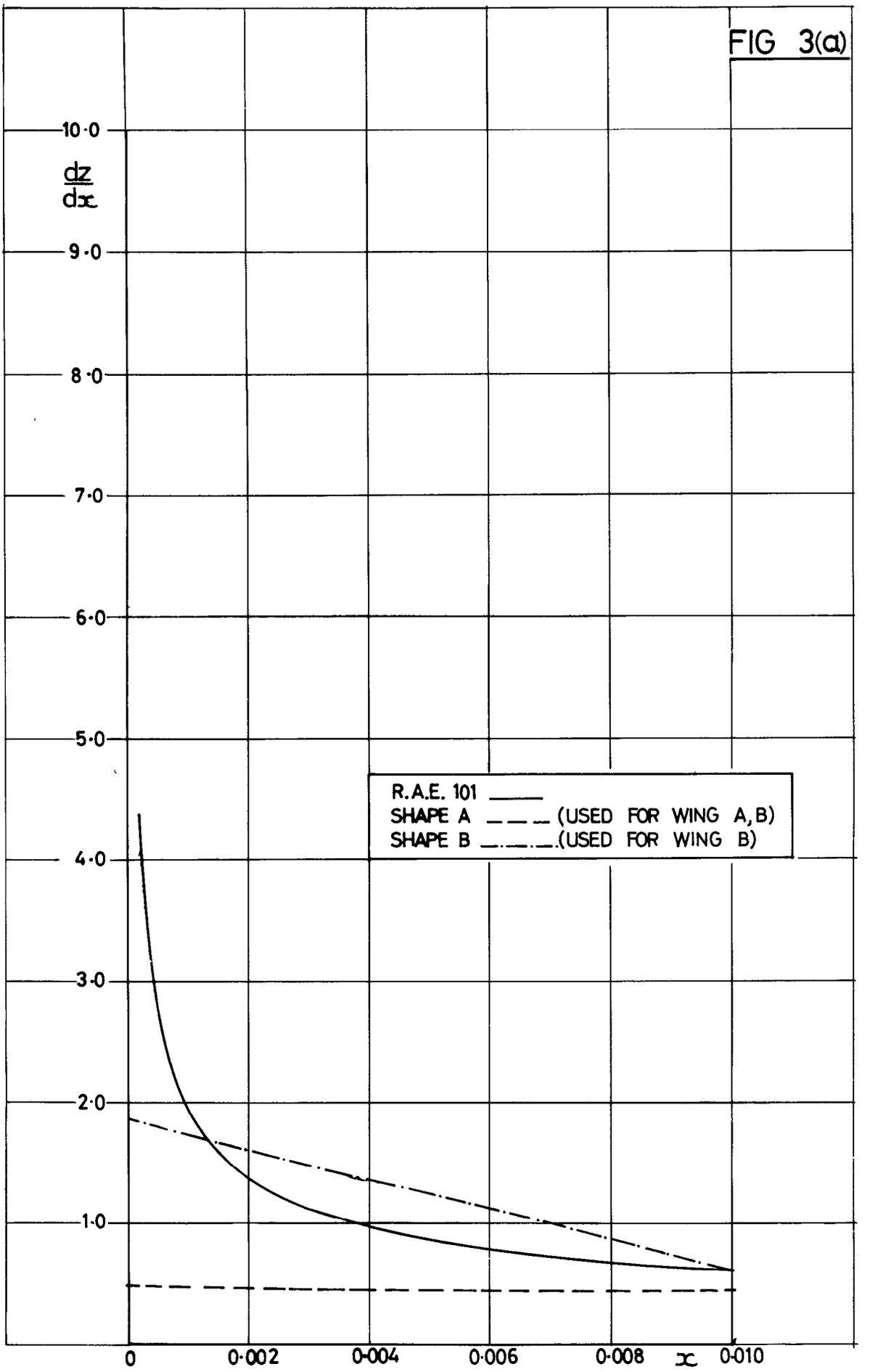

FIG 3(a) SLOPES OF SECTIONS USED FOR CALCULATIONS FOR WINGS A AND B

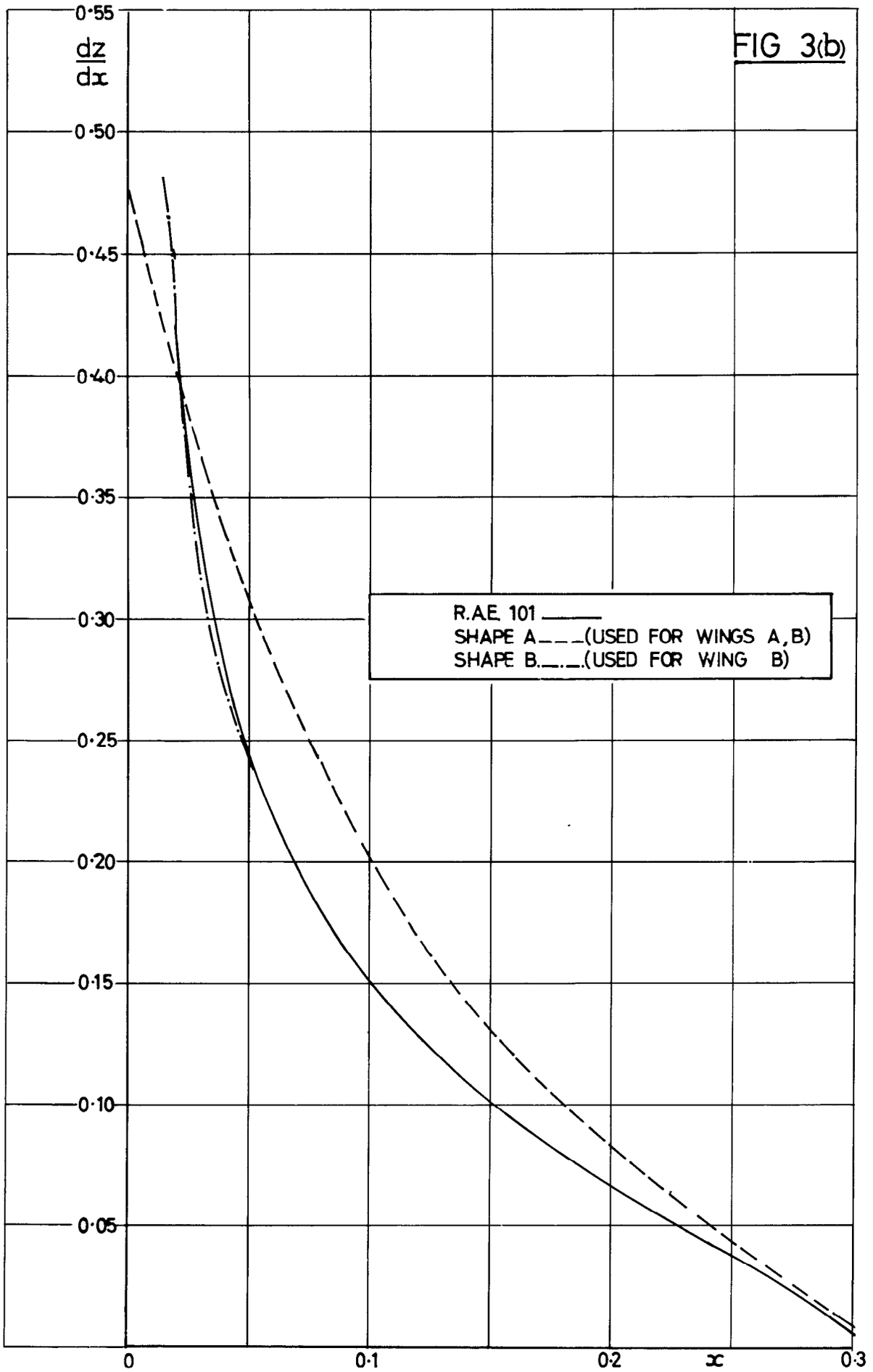

FIG. 3(b) SLOPES OF SECTIONS USED FOR CALCULATIONS FOR WINGS A AND B

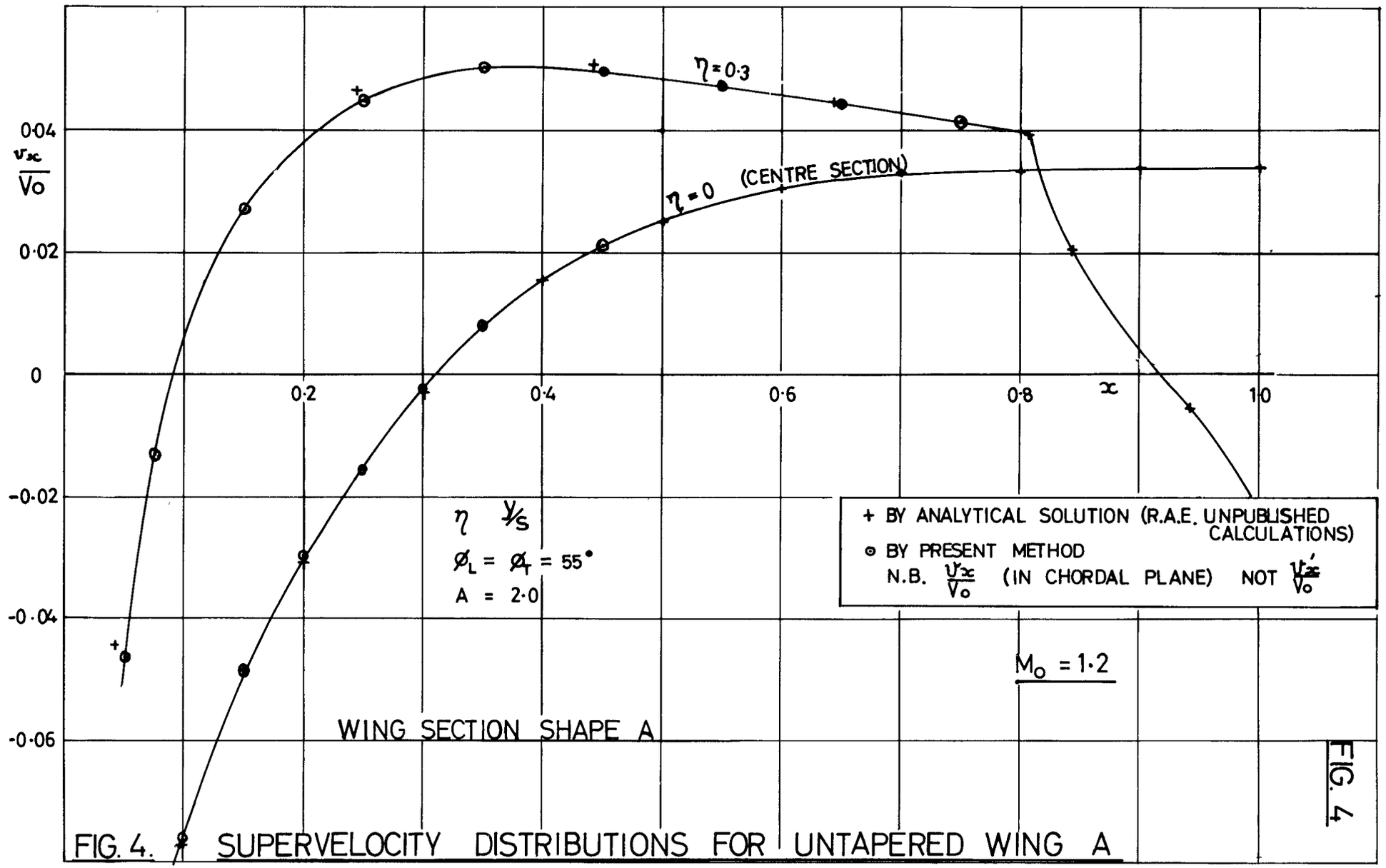

FIG. 4. SUPERVELOCITY DISTRIBUTIONS FOR UNTAPERED WING A

FIG. 4

FIG.5.

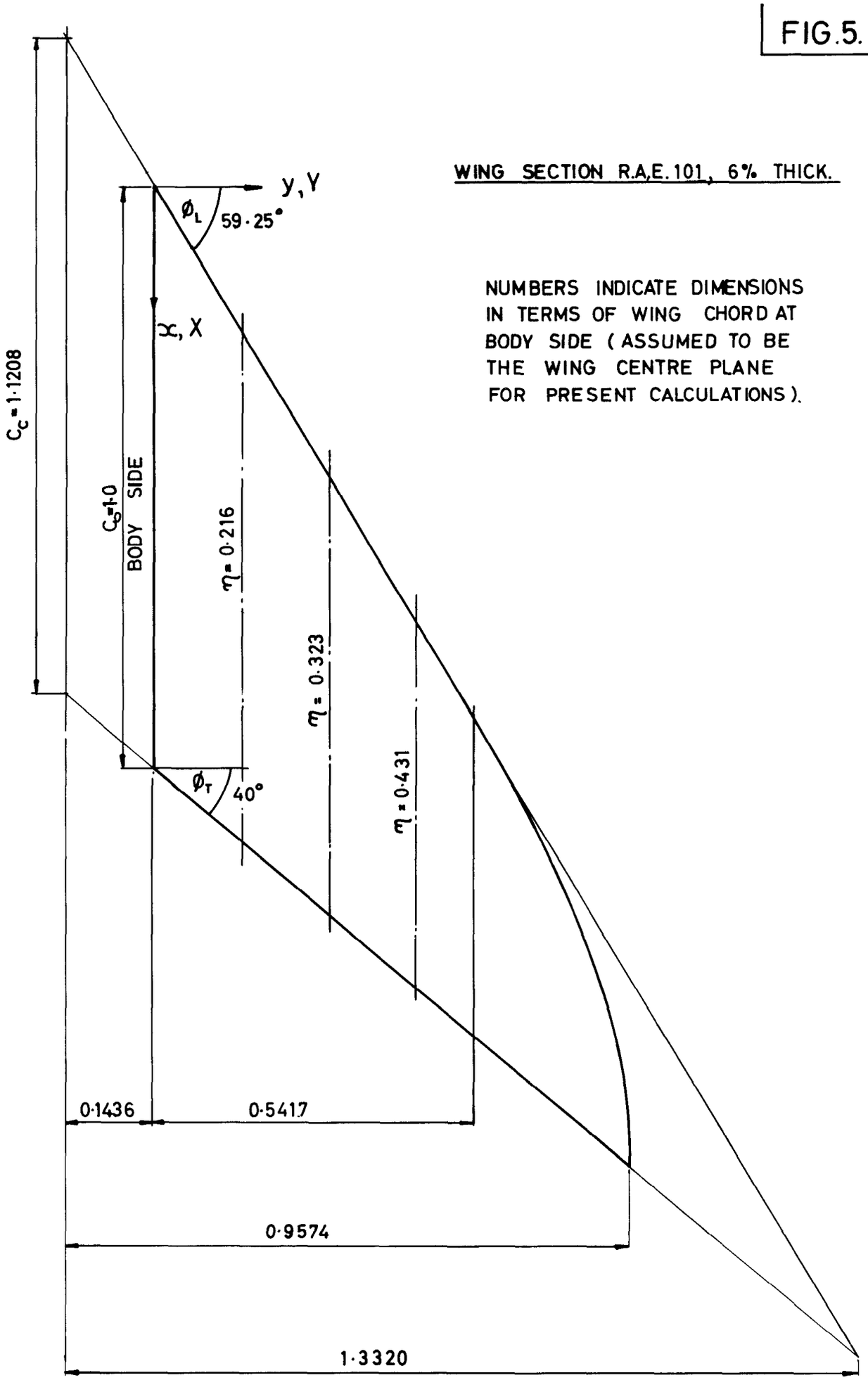

FIG. 5. PLAN GEOMETRY OF TAPERED WING B.

(SEE § 5·2)

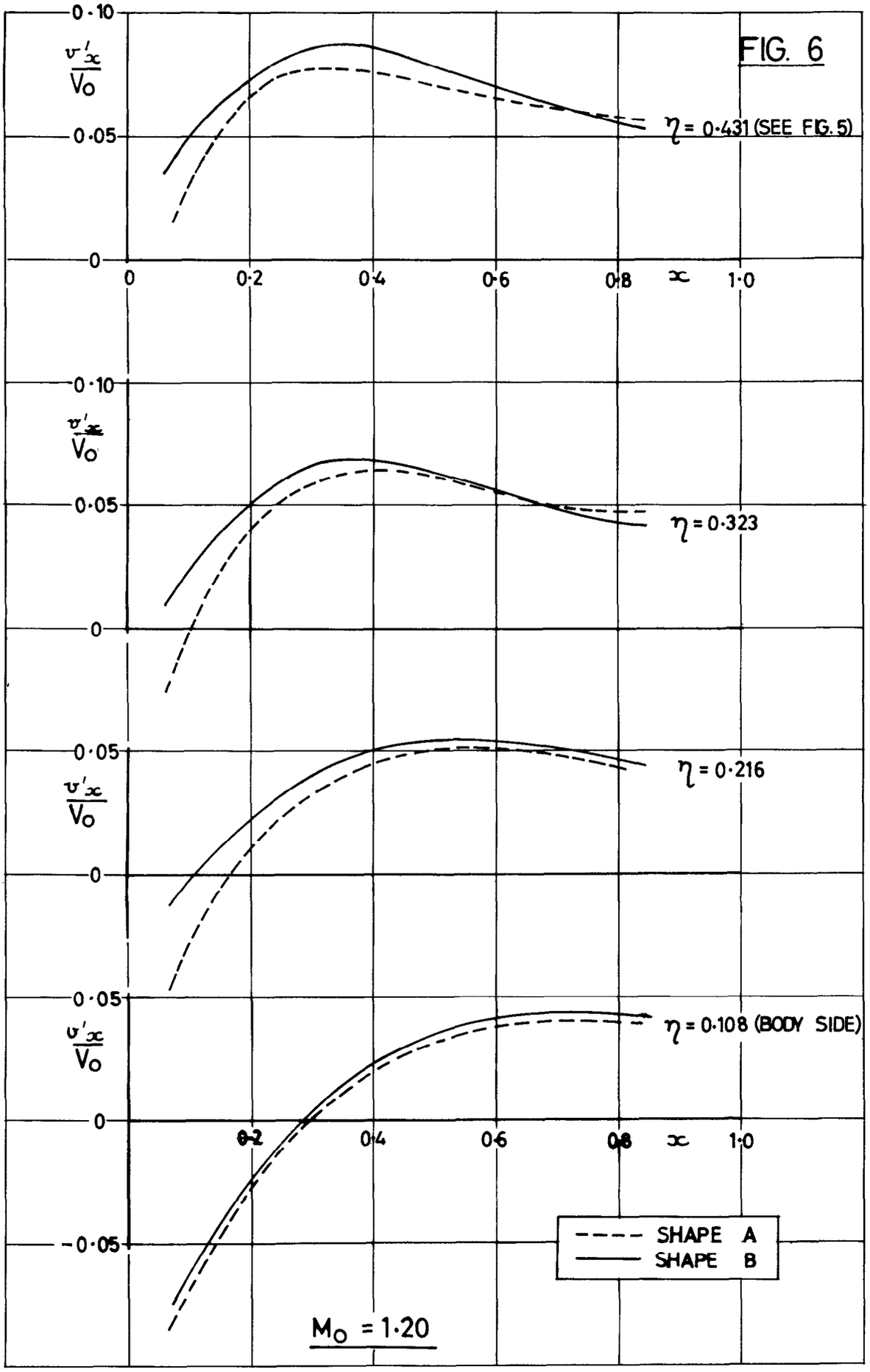

FIG.6. SUPERVELOCITY DISTRIBUTIONS FOR TAPERED WING B

EFFECT OF DIFFERENT SECTION SHAPES.

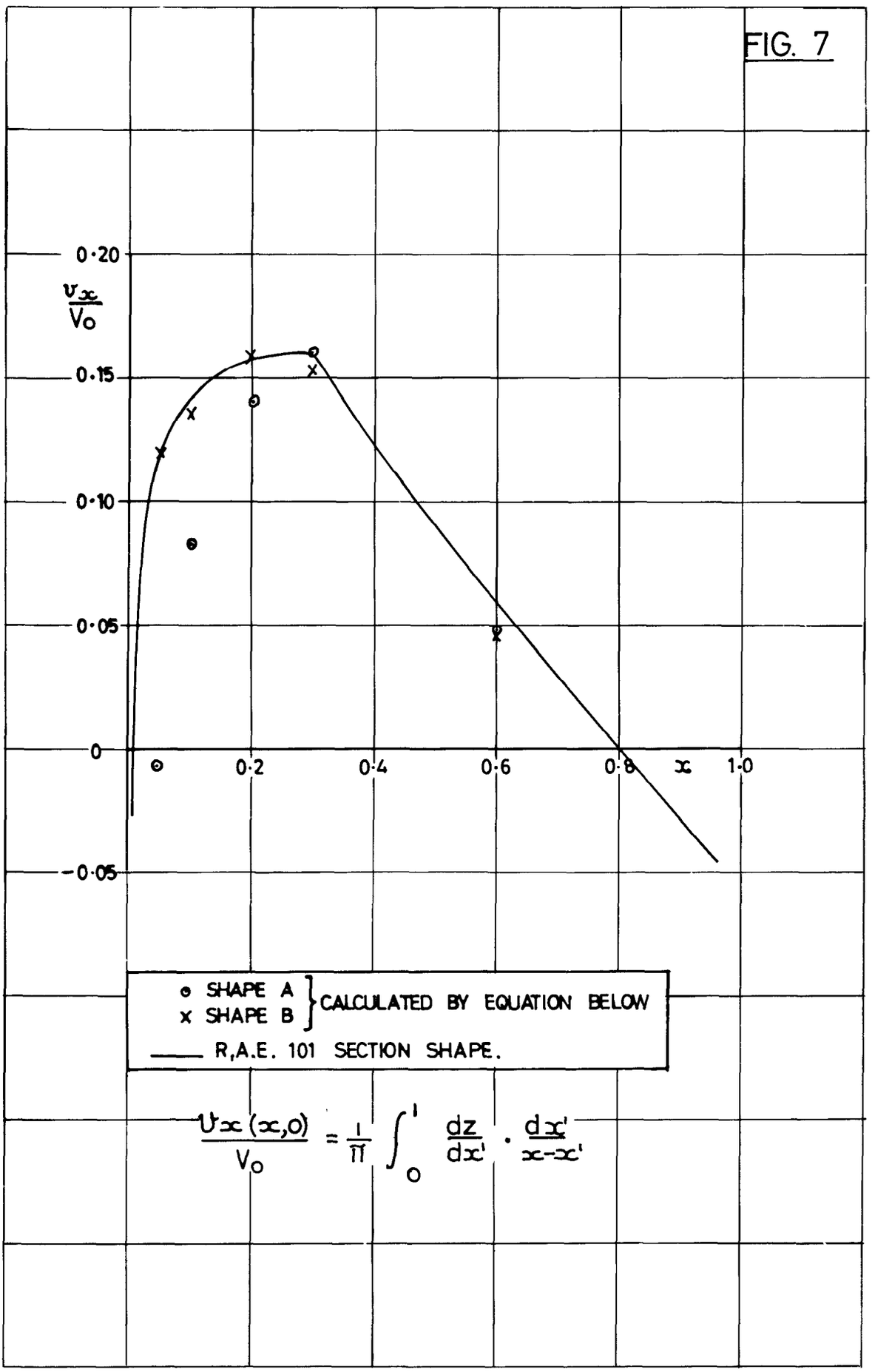

FIG. 7 COMPARISON OF VELOCITY DISTRIBUTIONS IN TWO DIMENSIONAL FLOW AT M = 0

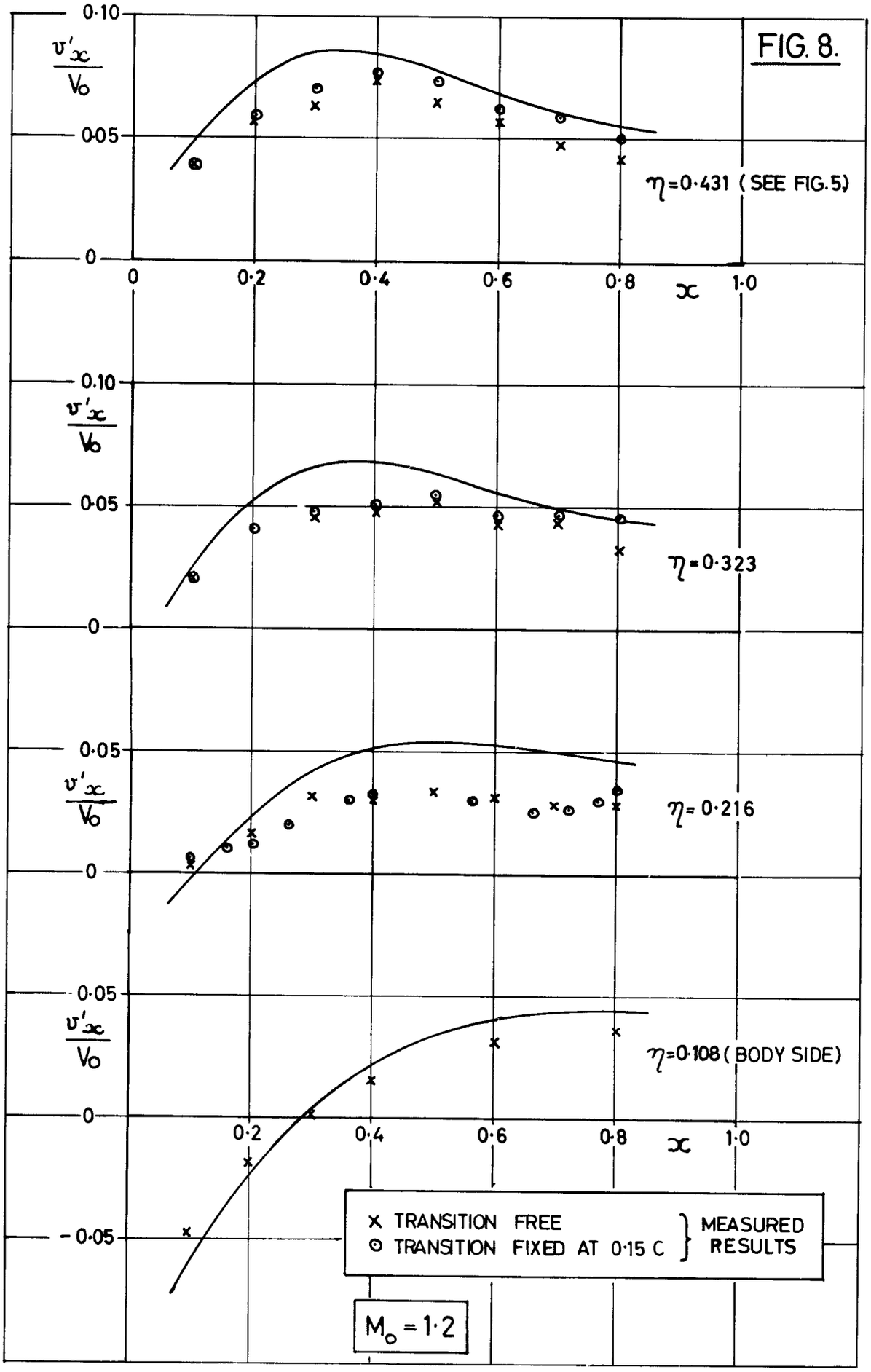

FIG. 8. SUPERVELOCITY DISTRIBUTIONS FOR TAPERED WING B.

COMPARISON OF CALCULATED AND MEASURED VALUES.

FIG. 9

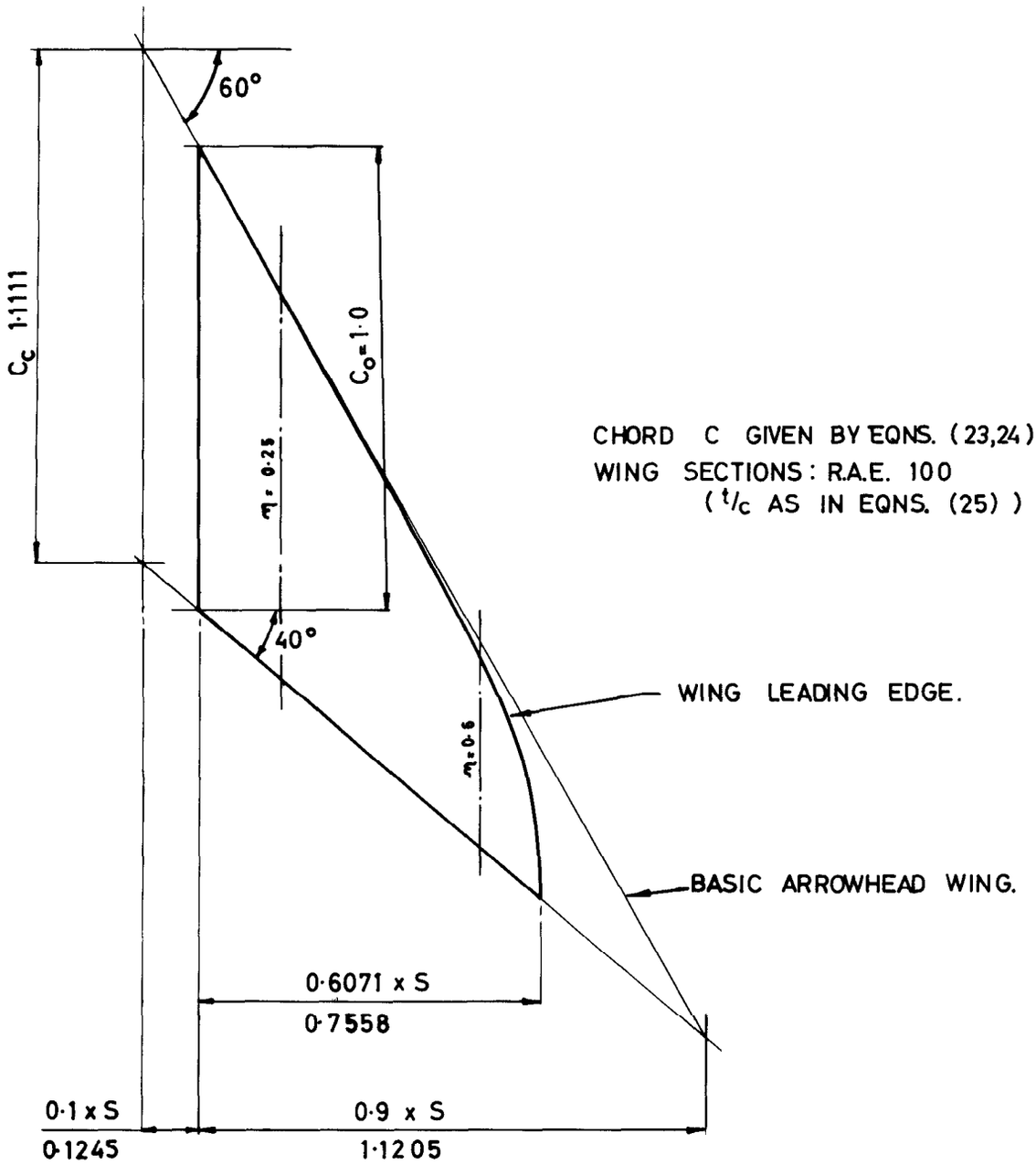

NUMBERS INDICATE DIMENSIONS IN TERMS OF WING CHORD AT BODY SIDE (ASSUMED TO THE WING CENTRE PLANE FOR PRESENT CALCULATIONS)

FIG. 9. PLAN GEOMETRY OF WING C WITH VARYING t/c ACROSS SPAN.

(SEE § 5·3)

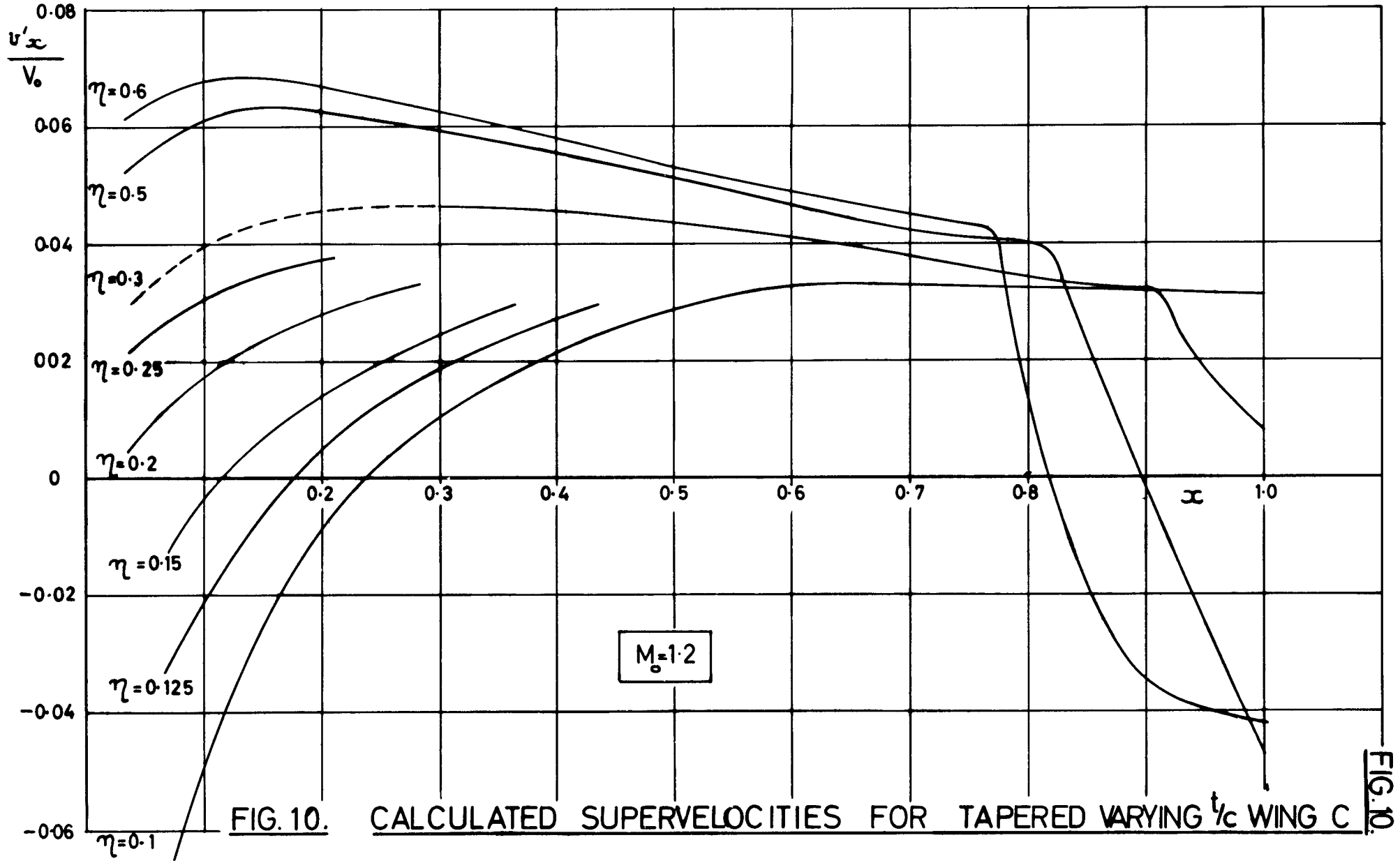

FIG. 10. CALCULATED SUPERVELOCITIES FOR TAPERED VARYING t/c WING C

FIG. 10.

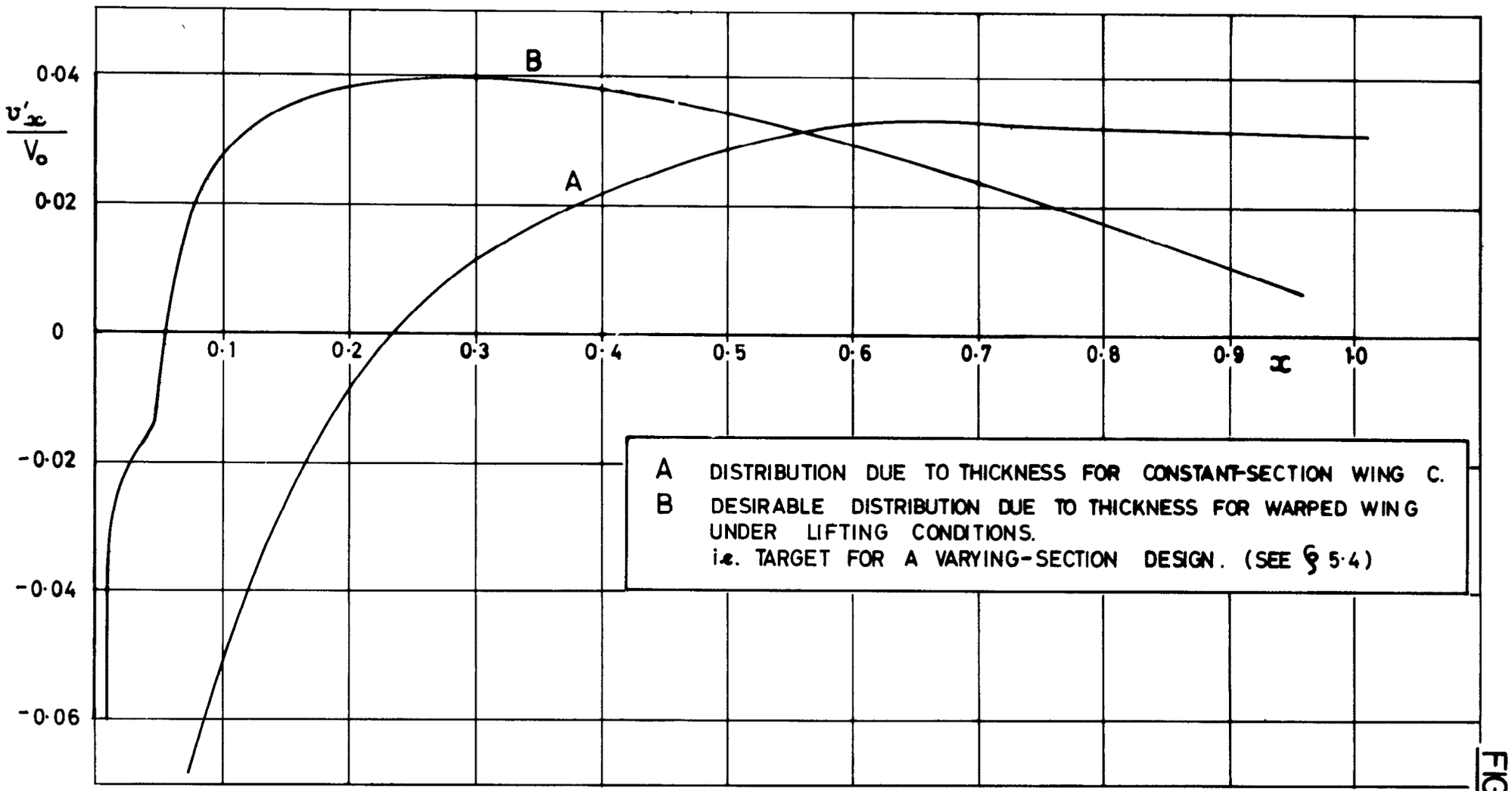

FIG. 11.

FIG. 11. BODY-SIDE DISTRIBUTION DUE TO THICKNESS $M_0 = 1{\cdot}20$.

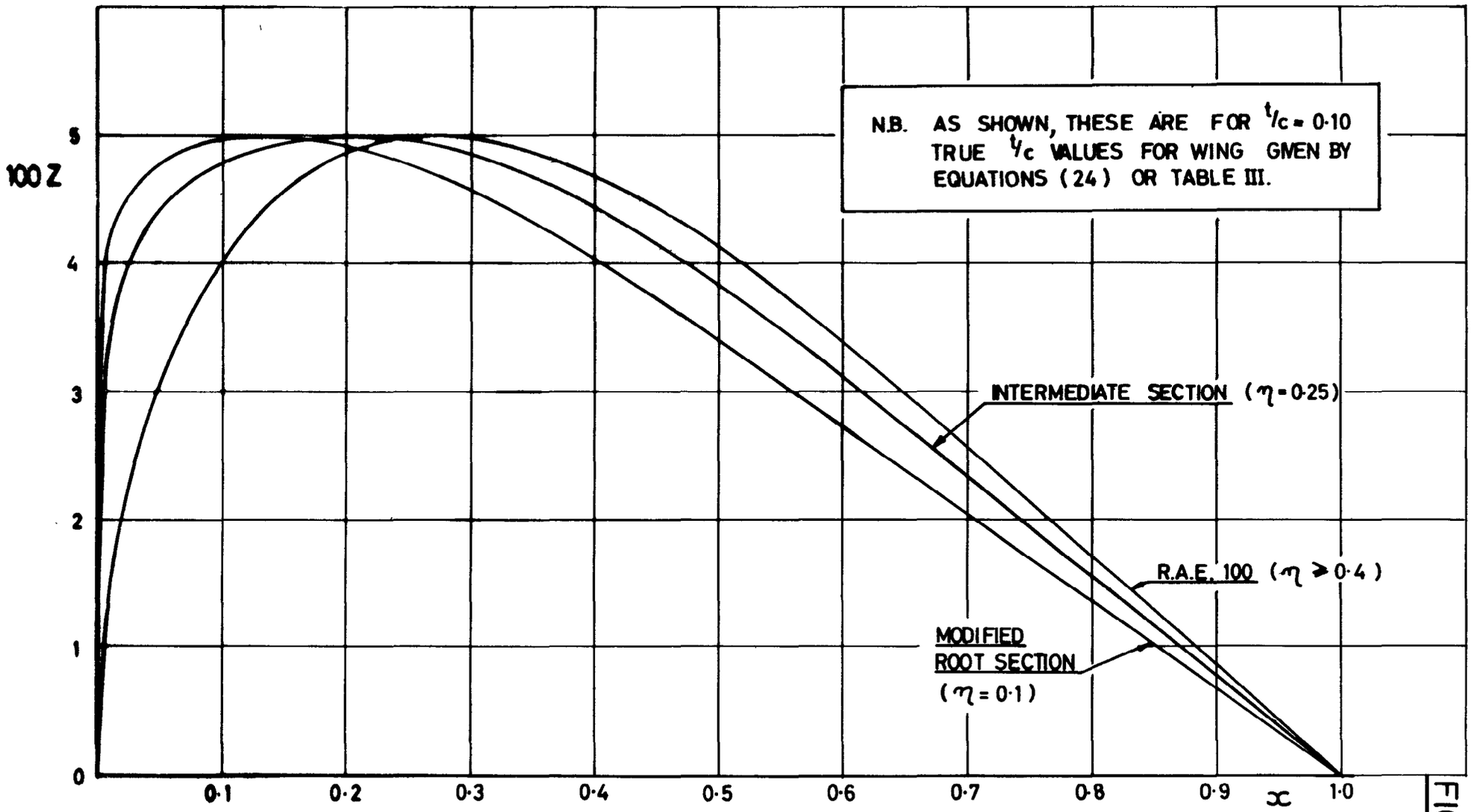

FIG. 12.

FIG. 12. SECTION SHAPES FOR VARYING SECTION WING D

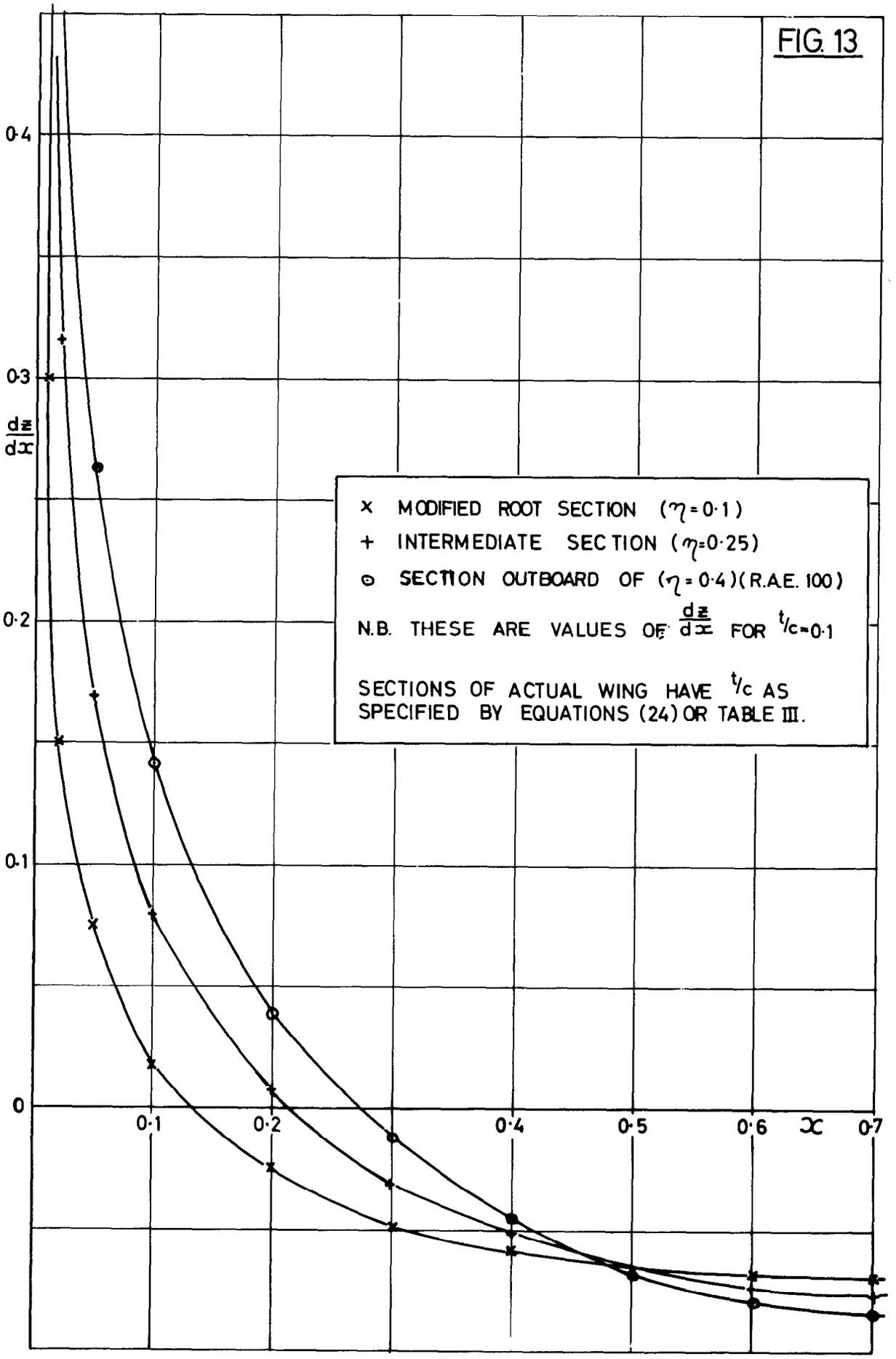

FIG. 13. SURFACE SLOPES OF VARYING SECTION WING D.

FIG.14.

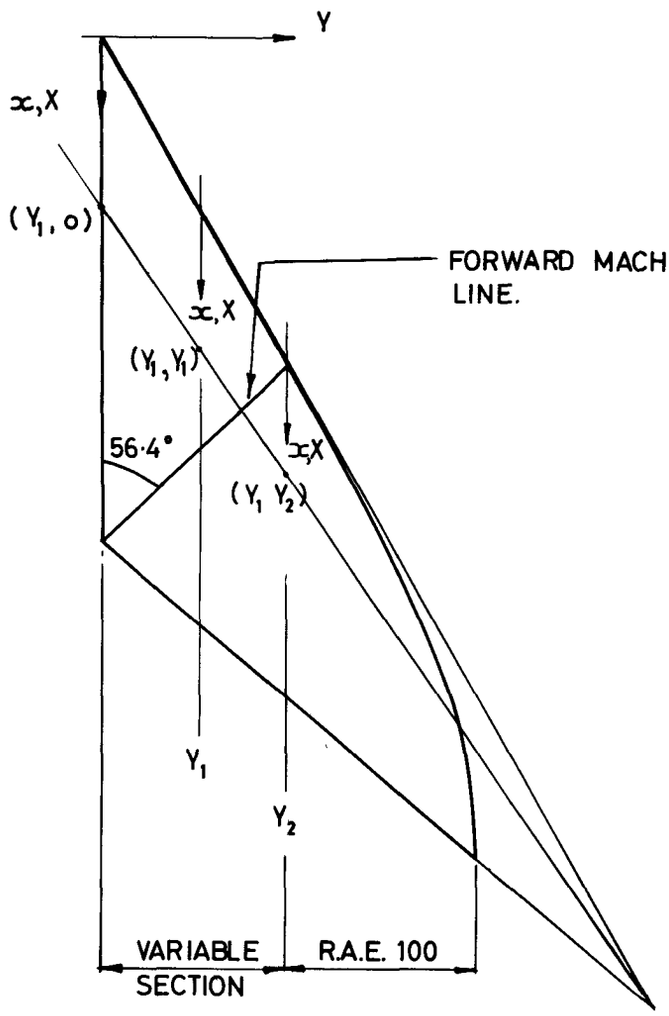

$$\left(\frac{\partial z}{\partial x} \times \frac{0{\cdot}1}{t/c}\right)_{X_1,Y_1} = \left(\frac{\partial z}{\partial x} \times \frac{0{\cdot}1}{t/c}\right)_{X_1,0} + \frac{Y_1}{Y_2}\left[\left(\frac{\partial z}{\partial x} \times \frac{0{\cdot}1}{t/c}\right)_{X_1,Y_2} - \left(\frac{\partial z}{\partial x} \times \frac{0{\cdot}1}{t/c}\right)_{X_1,0}\right]$$

Y DEFINED AS USUAL (FIG 1)

x, X = 0 AT LOCAL WING LEADING EDGE.

x, X, z NON-DIMENSIONALIZED IN TERMS OF LOCAL CHORD.

FIG. 14. METHOD ADOPTED FOR INTERPOLATING WING SECTION SHAPES ON WING D.
(PLANFORM AND t/c DISTRIBUTION AS FOR C)

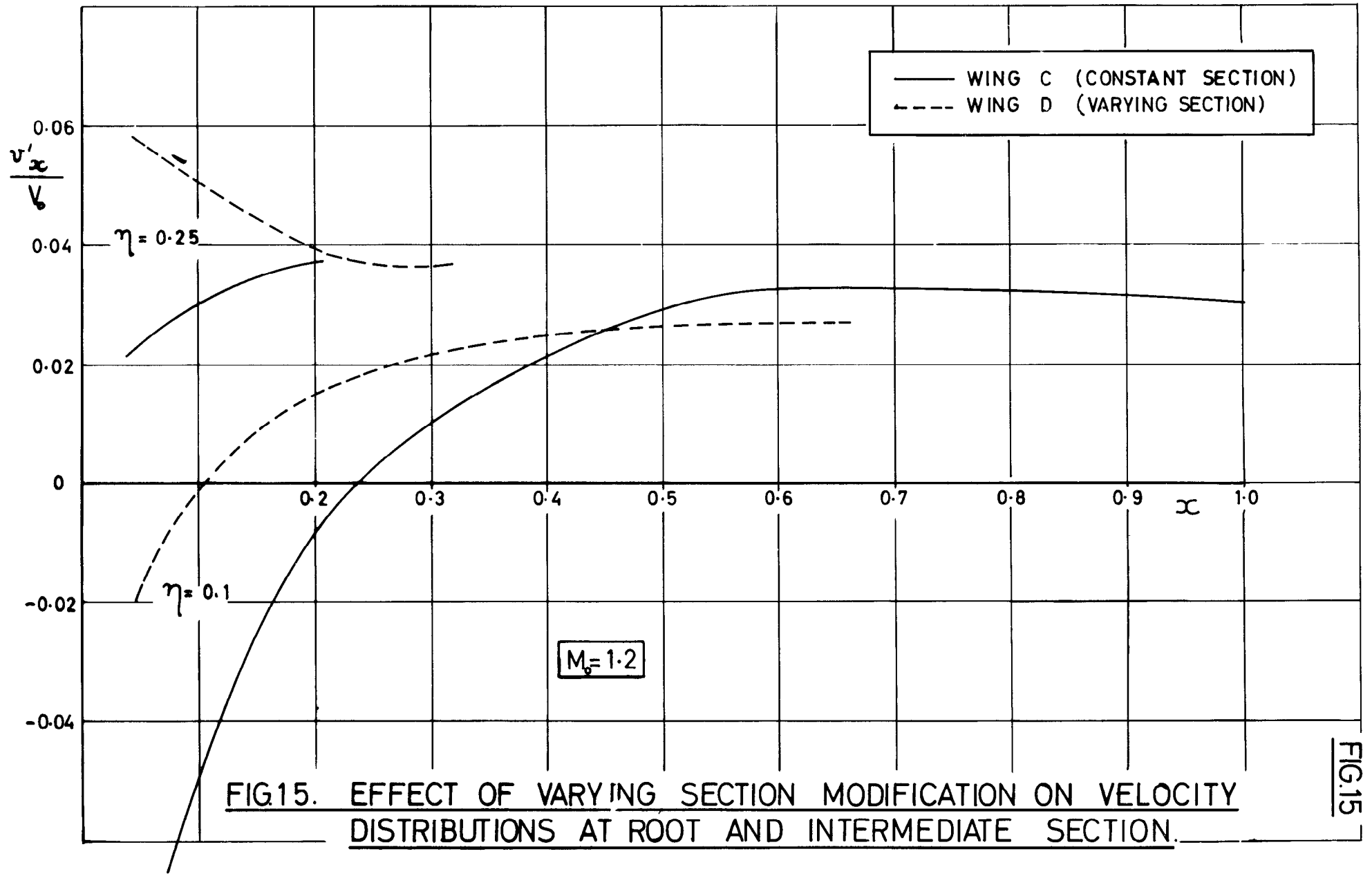

FIG.15. EFFECT OF VARYING SECTION MODIFICATION ON VELOCITY DISTRIBUTIONS AT ROOT AND INTERMEDIATE SECTION.

FIG.15

D 74728/1/Wt. 59 K 4 12/63 XL/CL

A.R.C. C.P. No.654. June, 1962.
Haines, A. B., Rollins, K. and Osborn, J.

THE CALCULATION OF THE VELOCITY DISTRIBUTION DUE TO THICKNESS FOR SWEPT WINGS WITH SUBSONIC EDGES AT SUPERSONIC SPEEDS

This note describes a method for calculating according to linearised theory, the velocities produced by the thickness form of a sweptback wing having subsonic leading and trailing edges at supersonic Mach numbers. The method has been programmed for the Zebra computer and can cope with wings of arbitrary planform having arbitrary variation of both thickness/chord ratio and section shape across the span. At present, the method will only deal with wings having sharp leading edges.

A.R.C. C.P. No.654. June, 1962.
Haines, A. B., Rollins, K. and Osborn, J.

THE CALCULATION OF THE VELOCITY DISTRIBUTION DUE TO THICKNESS FOR SWEPT WINGS WITH SUBSONIC EDGES AT SUPERSONIC SPEEDS

This note describes a method for calculating according to linearised theory, the velocities produced by the thickness form of a sweptback wing having subsonic leading and trailing edges at supersonic Mach numbers. The method has been programmed for the Zebra computer and can cope with wings of arbitrary planform having arbitrary variation of both thickness/chord ratio and section shape across the span. At present, the method will only deal with wings having sharp leading edges.

A.R.C. C.P. No.654. June, 1962.
Haines, A. B., Rollins, K. and Osborn, J.

THE CALCULATION OF THE VELOCITY DISTRIBUTION DUE TO THICKNESS FOR SWEPT WINGS WITH SUBSONIC EDGES AT SUPERSONIC SPEEDS

This note describes a method for calculating according to linearised theory, the velocities produced by the thickness form of a sweptback wing having subsonic leading and trailing edges at supersonic Mach numbers. The method has been programmed for the Zebra computer and can cope with wings of arbitrary planform having arbitrary variation of both thickness/chord ratio and section shape across the span. At present, the method will only deal with wings having sharp leading edges.

DETACHABLE ABSTRACT CARDS

e

o

.

It is likely however that for round-nosed sections, if the true section is replaced by an equivalent sharp-nosed section, reliable results may still be obtained, at least aft of about 0.04c.

Calculations have been made for the velocities due to thickness at M = 1.2 over four different wings. These are respectively, untapered, tapered in plan, tapered both in plan and thickness chord ratio and finally, tapered with a spanwise variation in section shape. In one case, a comparison with experimental results is given.

It is likely however that for round-nosed section, if the true section is replaced by an equivalent sharp-nosed section, reliable results may still be obtained, at least aft of about 0.04c.

Calculations have been made for the velocities due to thickness at M = 1.2 over four different wings. These are respectively, untapered, tapered in plan, tapered both in plan and thickness/chord ratio and finally tapered with a spanwise variation in section shape. In one case, a comparison with experimental results is given.

It is likely however that for round-nosed sections, if the true section is replaced by an equivalent sharp-nosed section, reliable results may still be obtained, at least aft of about 0.04c.

Calculations have been made for the velocities due to thickness at M = 1.2 over four different wings. These are respectively, untapered, tapered in plan, tapered both in plan and thickness/chord ratio and finally tapered with a spanwise variation in section shape. In one case, a comparison with experimental results is given.

Printed and published by
HER MAJESTY'S STATIONERY OFFICE

To be purchased from
York House, Kingsway, London W.C.2
423 Oxford Street, London W.1
13A Castle Street, Edinburgh 2
109 St. Mary Street, Cardiff
39 King Street, Manchester 2
50 Fairfax Street, Bristol 1
35 Smallbrook, Ringway, Birmingham 5
80 Chichester Street, Belfast 1
or through any bookseller

Printed in England